AD_____

Award Number: DAMD17-00-1-0599

TITLE: High-Resolution Speckle-Free Ultrasound Imaging System— A Potential Solution for Detecting Missed Breast Cancer

PRINCIPAL INVESTIGATOR: Matthew Freedman, M.D.

CONTRACTING ORGANIZATION: Georgetown University Medical Center
Washington, DC 20057

REPORT DATE: October 2005

TYPE OF REPORT: Final

PREPARED FOR: U.S. Army Medical Research and Materiel Command
Fort Detrick, Maryland 21702-5012

REPORT DOCUMENTATION PAGE

Form Approved
OMB No. 0704-0188

1. REPORT DATE	2. REPORT TYPE	3. DATES COVERED
01--2005		2004 – 2005

4. TITLE AND SUBTITLE
High-Resolution Speckle-Free Ultrasound Imaging System— A Potential Solution for Detecting Missed Breast Cancer

5a. CONTRACT NUMBER

5b. GRANT NUMBER
W81XWH-

5c. PROGRAM ELEMENT NUMBER

6. AUTHOR(S)
Matthew Freedman, M.D.

5d. PROJECT NUMBER

5e. TASK NUMBER

5f. WORK UNIT NUMBER

7. PERFORMING ORGANIZATION NAME(S) AND ADDRESS(ES)
Georgetown University Medical Center
Washington, DC 20057

8. PERFORMING ORGANIZATION REPORT NUMBER

9. SPONSORING / MONITORING AGENCY NAME(S) AND ADDRESS(ES)
U.S. Army Medical Research and Materiel Command
Fort Detrick, Maryland 21702-5012

10. SPONSOR/MONITOR'S ACRONYM(S)

11. SPONSOR/MONITOR'S REPORT NUMBER(S)

12. DISTRIBUTION / AVAILABILITY STATEMENT
Approved for Public Release; Distribution Unlimited

13. SUPPLEMENTARY NOTES

14. **ABSTRACT**
The Imperium Inc transmission ultrasound system is a highly promising novel method for imaging the breasts. In this pilot project, we worked with Imperium to advise and help them modify their existing system for non-destructive testing into one suitable for breast imaging. Technical development of the system took longer than originally anticipated. We have performed a series of physics tests. We have imaged pieces of animal tissue obtained in a supermarket We have performed a small pilot feasibility trial in human specimens. The initiation of this project was delayed by non-approval of the human use portion of the project, but we did receive US Army Human Use approval for study of human breast tissue samples and have studied 12. We are about to place the prototype system in the clinical breast center to study breast biopsy specimens with Imperium and standard ATL ultrasound. Imperium has continued to improve the machine during this past year. A prototype system for in vivo breast imaging has been designed with all but one major component constructed. The National Institute for Biomedical Imaging and Bioengineering (NIBIB) has recently provided to the Georgetown research team two years of new funding to continue this research.

15. SUBJECT TERMS
Detection breast cancer, C-Scan ultrasound, CCD coupled Piezoelectric sensor, ultrasound lens

16. SECURITY CLASSIFICATION OF:			17. LIMITATION OF ABSTRACT	18. NUMBER OF PAGES	19a. NAME OF RESPONSIBLE PERSON
a. REPORT	b. ABSTRACT	c. THIS PAGE			USAMRMC
U	U	U	UU	55	19b. TELEPHONE NUMBER *(include area code)*

Table of Contents

High-Resolution Speckle-Free Ultrasound Imaging System--A potential solution for detecting missed beast cancer

Introduction

The Imperium Inc. transmission ultrasound system is a highly promising novel method for imaging the breast. The system differs from traditional ultrasound in that it transmits the ultrasound beam through the breast and records the ultrasound transmitted through tissue rather than the reflection of the ultrasound by tissue. Because the properties of tissue to ultrasound differ for reflection and transmission, this new method may provide new information about breast and breast tumor composition. In this pilot project, we worked with Imperium to advise and help them modify their existing system for non-destructive testing into one suitable for breast imaging, performed a physics evaluation of the system and performed a small feasibility trial in fresh and quick frozen and then thawed human breast tissue specimens. The initiation of this project was delayed by non-approval of the human use portion of the project because of disagreements between requirements of the US Army Breast Cancer Program's Human Subjects reviewers and those of Georgetown University's Institutional Review Board. We did finally receive approval from both to study human biopsy specimens. Once approval was given, I delayed the imaging of human tissue until I felt the system was ready. The latest version of the system, delivered in June, 2005, was of appropriate quality and we started human tissue imaging. 12 samples have been imaged to date. The initial prototype system (shown below) for in vivo human imaging lacked important ergonomic features and on initial tests in phantoms was not suitably designed (the breast tissue was not adequately supported and appeared likely to slide from the machine). This has been redesigned and will be delivered to us shortly for in vivo testing. While development of the system took longer than anticipated due to the engineering complexity, we remain strongly interested in this system and believe in its eventual success. The preliminary data from this project was used in a submission to NIH for additional funding and we were recently awarded two years of funding from The National Institute for Biomedical Imaging and Bioengineering (NIBIB) to continue development of the system and for a small in vivo clinical trial.

Body

During this project we have worked closely with our subcontractor, Imperium, Inc. on the development of the imaging system and its physics and animal tissue testing. These tests are described below. Much of this work was done in water baths to permit the more rapid exchange of parts. In response to the results shown in the images, we and Imperium discussed methods for the improvement of the machines that were progressively made and incorporated into the laboratory prototype. Results from the initial and current machine are compared below. During this work, two different prototypes for in vivo breast imaging were constructed. Tests of the first showed that it was not completely suitable. The second prototype system for in vivo imaging appears more promising, with initial deficits corrected, but still needs to be tested. We accompanied the company when they had an informal conference with the FDA. This was done to start their learning process of the requirements for eventual FDA approval. Safety information from the physics testing was extensively discussed during the FDA meeting and the FDA appears to have no safety concerns; however, this was an informal meeting with their ultrasound specialist scientists and regulatory experts for ultrasound devices, rather than a formal submission.

The following represents a combined presentation of work done by Imperium, Inc. and Georgetown in testing the system prior to its use in human tissue specimens.

The laboratory research system is a water bath system. Two different dry systems have been constructed for eventual in vivo breast imaging and are described later.

The Water Bath System:

To generate real-time images, ultrasound is introduced into the target under study with a large unfocused ultrasound plane wave. The resultant pressure wave strikes the target and is attenuated and scattered. An acoustic lens collects the energy and focuses it onto the ultrasound sensitive array. The array is made up of two components, a silicon detector/readout array and a piezoelectric material that is deposited onto the array through semiconductor processing (see Figure 1). The array is 1 cm on a side consisting of 128×128 pixel elements (16,384) with 85μm pixel spacing. The energy that strikes the piezoelectric material is converted to an analog voltage that is digitized and processed by low cost commercial video electronics.

Note that there is an ultrasound-receiving (piezoelectric) layer deposited onto the chip. A picture of the microarray is shown in Figure 2. The array is responsive over a wide range of ultrasound frequencies, although most imaging is done between 1MHz and 10MHz. The use of a lens provides a simple, inexpensive alternative to complex beam forming often employed in ultrasound imaging. The user simply focuses by adjusting the lens while looking at the image on a monitor. Figures 3 and 4 show the overall system configuration and the laboratory setting in a water tank, respectively.

The original system operated by pulsing a commercial off-the-shelf ultrasonic spike pulser in 5 MHz frequencies. The system has been tested as well at 7.5 and 10 MHz providing higher resolution, but with decreased penetration through tissue. The ultrasound spike pulser excites the large area unfocused ultrasound transducer (only used as a source) and sends an ultrasound plane wave through the water. This plane wave enters the target, scatters, exits the target and strikes the acoustic lens, which collects the scattered energy and focuses it onto the array. This operation repeats 30 times/second to generate real-time image. Standard video electronics and image processing are used to format the image for presentation to the user and perform real time image processing; either on a PC monitor or LCD.

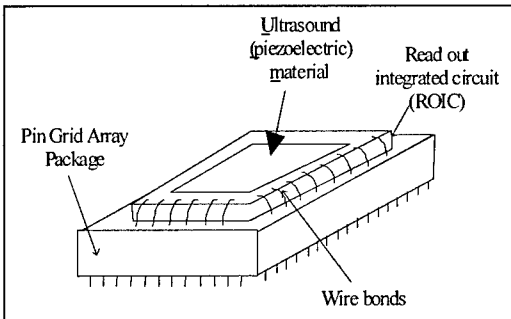

Figure 1. Schematic of array assembled array

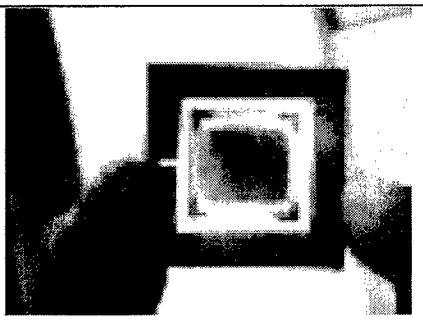

Figure 2. 128 × 128 assembled array

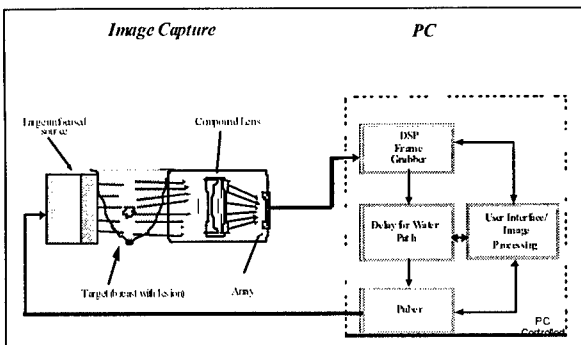

Figure 3. The prototype system configuration

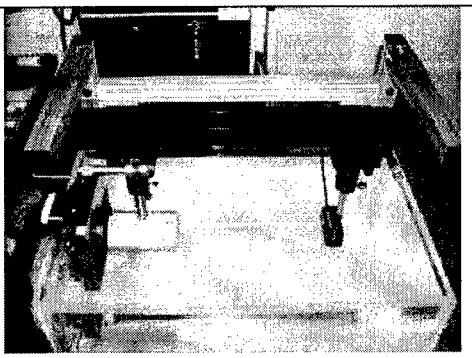

Figure 4. Laboratory setting in a water tank

Contrast Resolution

The ability of the camera to resolve separate tissue layers is a function of its sensitivity to small changes in amplitude. We tested the camera's ability to resolve these small differences in detected signal level. The phantom used in this investigation was a custom-made Zerdine™-based phantom containing 3-mm and 5-mm spheres with small differences in attenuation from the surrounding background material. The phantom was manufactured by Computerized Imaging Reference Systems Inc. (CIRS, Norfolk, VA). The background material has an attenuation of 0.22 dB/cm/MHz that approximates the attenuation of fatty tissue [1, Table 4.6]. Two of the spheres were slightly less attenuating than the background and two of the spheres are slightly more attenuating than the background.

The ability to resolve amplitude differences is measured by calculating a Contrast to Noise Ratio (CNR), given by $CNR = (I_s - I_b)/\sqrt{(\sigma_s^2 + \sigma_b^2)/2}$, where the I_s and I_b are sphere and background mean intensities and σ_s and σ_b are the respective standard deviations. In these measurements, statistics for a block of image pixels inside and outside each sphere area were collected and analyzed. Transmission images were obtained with an Imperium I-100 camera, a two-element aspheric 50 mm diameter F/1 (Imperium 915 series), and a 5.4-MHz center frequency, 1.5 in. diameter pulsed transducer. Figure 5 shows the images taken of this phantom.

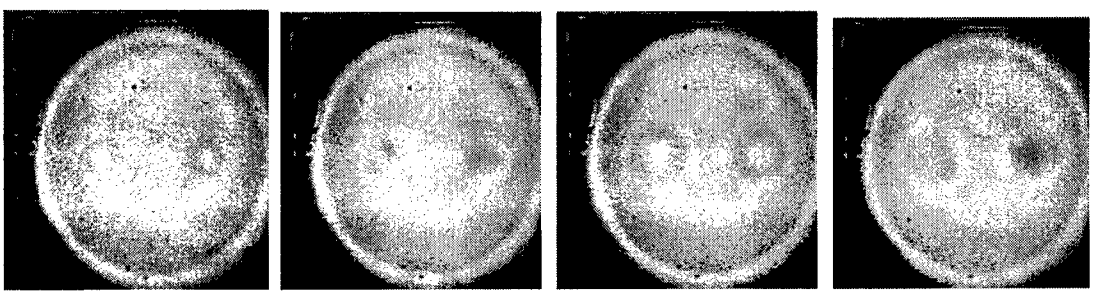

3 mm	3 mm	5 mm	5 mm
0.06dB, 0.15dB	0.5dB, 0.8dB	0.06dB, 0.15dB	0.5dB, 0.8dB

Figure 5 Transmission images of the CIRS contrast phantom.

The sphere diameters and their attenuations (dB/cm/MHz) are indicated in Figure 5. The overall circular field of view indicates the beam diameter. Note the edges around the spheres. The pronounced edges are caused by the refraction edge effect that tends to enhance object resolvability. This effect is known as phase

contrast in gapped projection images [2]. We have described this phenomenon and its possible role in enhancing contrast mammography [3]. This refraction edge effect is one clear difference between conventional ultrasound and transmission ultrasound since this effect does not occur with reflection ultrasound. It allows one to evaluate the relative characteristics of the nodule of interest to the surrounding tissue. Thus the simulated cysts appear black with a white rim and the simulated solid nodules are white with a black rim. We expect that these rims may enhance the conspicuity of small solid nodules imaged with the novel transmission ultrasound, but do not yet know what the effect on normal breast tissues will be.

The results of the CNR calculations are shown in Table 1. Note that there are 256 grayscale levels to represent pixel intensities. This phantom was designed to mimic the breast with embedded cysts and solid masses. The spheres with attenuation less than the background material mimic cysts in this phantom. The spheres with attenuation greater than the background material mimic solid masses.

Table 1
Contrast Resolution

Sphere	Size (mm)	Differential Attenuation (dB)	Sphere Mean Intensity	Sphere Std. Dev.	Back-ground Mean Intensity	Back-ground Std. Dev.	Contrast	CNR
1	3	0.26	199	17	152	14	47	3.02
2	3	0.12	179	13	152	14	27	2.00
3	3	-0.45	117	11	154	16	-37	-2.69
4	3	-0.94	111	8	154	16	-43	-3.40
5	5	0.44	225	19	149	17	76	4.22
6	5	0.19	166	12	149	17	17	1.16
7	5	-0.75	138	12	157	17	-19	-1.29
8	5	-1.56	99	9	157	17	-58	-4.26

The contrast and CNR calculated in Table 1 must be viewed in the context of the amount of material contributed by the background and by the spheres. The attenuation of the background material is 0.22 dB/cm/MHz, the width of the phantom is 6 cm, and the center frequency of the transducer output is 5.4 MHz. The total attenuation through the phantom where there is no sphere is 7.13 dB. The differential attenuation column indicates the absolute difference between a phantom volume with no sphere and the phantom volume with spheres of different sizes and densities. The differential attenuation column in Table 1 is valid though the center of the sphere. Attenuation through off center sphere volumes will be closer to the background because there is less sphere material. It is notable that objects are resolvable with attenuation differences as small as 0.12 dB.

To determine the relative relevance of this phantom to imaging tissues, we have imaged mouse mammary glands discarded from other experiments because they had not developed tumors.

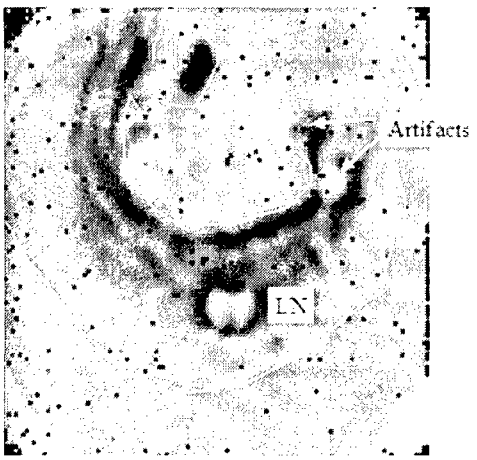

Figure 6. This figure shows an Imperium ultrasound image and a photograph of an isolated mouse mammary gland (gland #4). This gland contains a lymph node (LN) within it that is easily seen on the ultrasound image. In addition, several curvilinear bands are seen within the ultrasound image. On the digital photograph we see vessels within the gland that correspond (most likely) to the light gray band running through the ultrasound image. The Imperium system does not provide measurement capabilities yet, but the overall length of this gland in the mouse is approximately 15 mm. Image was made at 10 MHz. Black dots are defective pixels. This is the first custom-made model of this new ultrasound detector. The lymph node is approximately 2-3 mm in diameter.

Dynamic Range

The dynamic range of the earlier system is set by the analog output of the camera and the 8-bit analog frame grabber used by the display system. The dynamic range of the next generation camera system (currently in prototype and undergoing testing) is expected to be greater than 70 dB. The next generation camera will incorporate a 14-bit analog/digital converter (ADC) that will preserve the fidelity of the detector array in the accumulation of raw ultrasound data. We expect that the ultrasound data will be compressed to 8-10 bits for video display. Image compression techniques will be used to enhance the contrast resolution of the desired image area. With the use of a variable power output from the ultrasound transducer it is expected that the total dynamic range of the next generation camera will be well over 100 dB.

Twelve images were collected from a custom-fabricated dynamic range step phantom supplied by CIRS. These images are shown in Figure 7. A background pixel intensity of 57 was calculated by observing an area of the display in which there was a de-bonding of the piezo-electric material from the detector array. In this area there is no energy added to the pixel cells from ultrasound detection. Figure 8 shows a graph of pixel intensity versus the attenuation step. Each attenuation step is 2.7 dB.

The images were obtained with an Imperium I-100 camera, a two-element aspheric 50 mm diameter F/1 (Imperium 915 series), a 3.85 MHz center frequency, 1.5" diameter pulsed transducer. The peak sound pressure amplitude output from the transducer was 1.45 MPa.

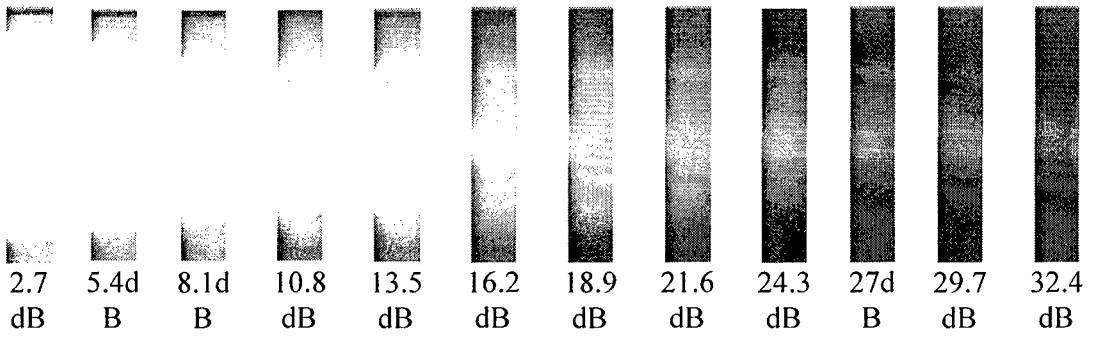

Figure 7. Twelve steps of the dynamic range phantom with associated attenuation @ 3.85MHz.

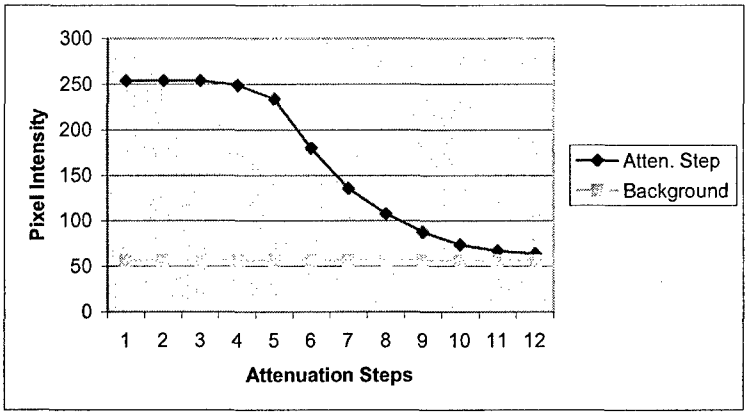

Figure 8 Dynamic Range of I100 Camera. Each attenuation step is 2.7 dB.

As a comment on the dynamic range performance, the camera was able to penetrate 32.4 dB of phantom material. The attenuation of the material at 0.70 dB/cm/MHz approximates that of the average for soft tissue ([1], pg. 51). The phantom is 17.1 cm or 6.84 in. thick at the 32.4 dB step, the current Imperium ultrasound camera should then be capable of penetrating more than 6 in. of soft tissue in its current configuration. Greater sensitivity is expected in the next generation of camera. In mammography, the normal compressed breast thickness varies from 3 to 8 cm depending on breast size and breast density. Thus the dynamic range results support the feasibility of using the Imperium camera for breast imaging (17 cm penetrating ability vs. 8 cm for maximum usual breast thickness).

The newer ultrasound detector has a wider dynamic range and uniformity of response as shown in the figure and table below.

5 MHz														
steps		0dB	4.95	9.9	14.85	19.8	24.75	29.7	34.65	39.6	44.55	49.5	54.45	59.4
Background	0.2	5.4	4.95	4.5	4.05	3.6	3.15	2.7	2.25	1.8	1.35	0.9	0.45	0.
Phantom	0.2	5.4	9.9	14.4	18.9	23.4	27.9	32.4	36.9	41.4	45.9	50.4	54.9	59.4
Total (dB)	**1.88**	**7.08**	**11.58**	**16.08**	**20.58**	**25.08**	**29.58**	**34.08**	**38.58**	**43.08**	**47.58**	**52.08**	**56.58**	**61.08**

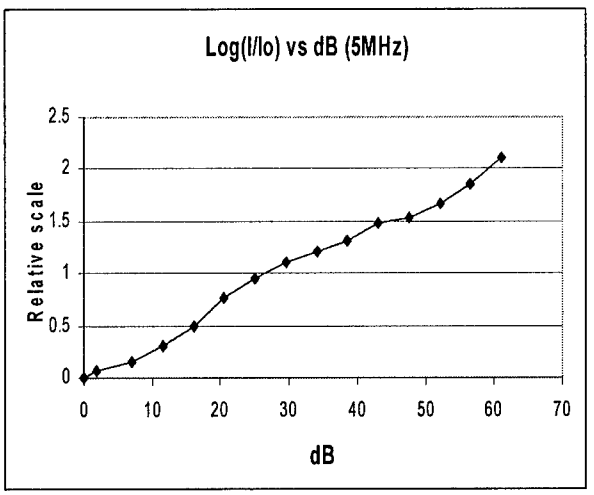

Figure 9: This demonstrates the wider dynamic range of the newly designed and made Imperium camera. This newly designed chip should greatly enhance the detection of abnormalities within breast tissues.

Spatial Resolution

The purpose of this task is to investigate the ability of the camera to resolve separate objects in a field of view, a function of its spatial resolution. The custom-fabricated Zerdine™-based CIRS phantom used in this investigation contains seven, 250 μm steel wires embedded in a fan shape. Transmission image data was obtained with an Imperium I-100 camera, a two-element aspheric 50 mm diameter F/1 (Imperium 915 series), and a 5.4-MHz center frequency, 1.5"-diameter pulsed transducer. Figure 9 shows an image taken of this phantom. Spatial resolution of the camera is determined by its ability to resolve the wires and the gaps between the wires.

The acoustic lenses designed by Imperium for its ultrasound cameras are diffraction limited.
Eq. (1) describes the limit of resolution for the diffraction-limited lens used in this investigation.

$$D_L = 1.22\lambda F/D \qquad \ldots(1)$$

$\lambda = 277$ μm (5.4 MHz)
D = diameter of the aperture = diameter of the transducer = 1.5 in. = 3.75 cm
F = Focal Length = 50 mm
$D_L = 451$ μm

The above computation indicates that the resolution of the system used for this investigation should be about 500 μm. Images shown in Figure 10 and results of work by Ishisaka et al [2] indicate that the phenomenon of phase contrast acts to enhance the edges of objects and may significantly improve the resolution achievable over the limit of Eq. 1.

Quantitative results of the first spatial resolution investigation are shown in Figure 11. The intensity of the steel wires is shown as the lower pixel values and the gaps between the wires are shown as the higher values. The center of the image in Figure 10 is 55 mm from the apex of the fan and the fan spreads at an angle of 4.77°. The distance between the outer two wires at the red line in Figure 10 is 9.17 mm. As can be seen, there is substantial blurring of the wires in the image. The aggregate width of seven, 250 μm wires is only 1.75 mm and so should account for only a small part of the width as seen in the image. The blurring is to be expected as the diameter of the wire is only half the spatial resolution predicted by Eq. 1. Observe that five of the six wire gaps are pronounced and one is obscured. This is due to an imperfection in the phantom. Two of the wires lay on top of each other.

The conclusion from this investigation is that we are limited by the operating frequency of the ultrasound camera. It is desirable that we should be able to resolve the 250 μm wires with no blurring. By doubling the frequency to 10 MHz it is predicted from Eq. 1 that we will be able to image the wires without blurring.

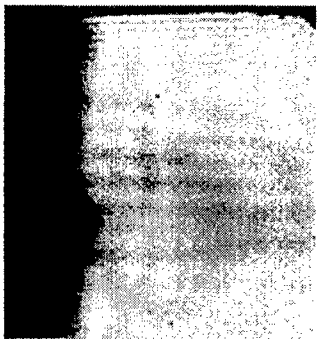

Figure 10 Wire Fan Phantom.

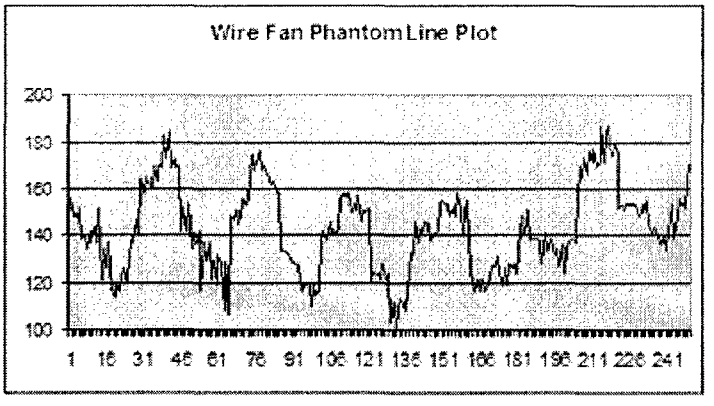

Figure 11 Fan Phantom Line Intensity Plot

A second spatial resolution test was conducted with a CIRS microcalcification phantom. It consisted of Zerdine™ material with imbedded calcium carbonate inclusions with diameters 150-160, 250-280, 320-355, 425-450, and 710-850 μm. Camera images are shown in Figure 12.

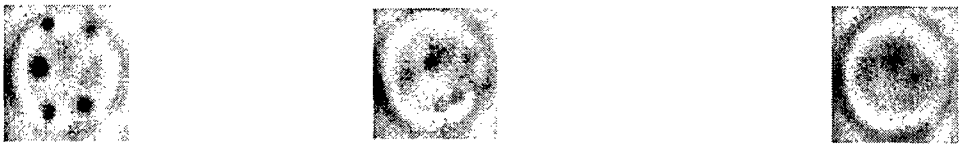

(a)710-850μm target group **(b)**425-450μm target group **(c)**300-355μm target group

Figure 12

Figure 12a clearly shows 700 μm targets. 700 μm is greater than the calculated resolution and thus it is expected that the targets will be easily seen. Figure 12b shows the presence of 450 μm targets but the resolvability of the targets is strained. A single target is clearly seen and other targets are less clearly seen.

Unfortunately, most of the targets in this phantom are placed on the lip of an Acrylic dish that holds the targets in place. This is unfortunate because there are refraction effects at the boundaries of this lip that make the targets hard to see. Figure 12c shows the presence of 300 μm targets. The targets in this phantom are blurred as would be expected when the targets are smaller than the resolution limit. We also evaluated the intensities of the calcification flecks in this phantom. The results are shown in figure 13.

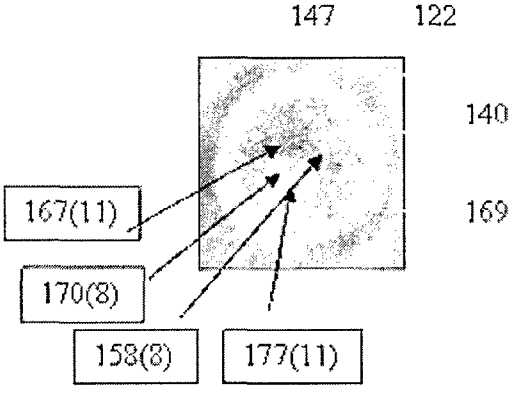

Figure 13: CIRS phantom with calfications ROIs and their intensities and CNRs measures for the smallest clustered calcifications. (A)Four intensity measures for the calcifications upper-right corners and the intensity (noise level) measures at selected background areas

Potential methods to improve resolution

From Eq. 1 it can be seen that resolution can be improved by increasing the frequency, decreasing the focal length, or increasing the diameter of the lens. Decreasing the focal length of the system used in this investigation is impractical. With a lens diameter of 50 mm and a focal length of 50 mm, the current design utilizes a F1 lens. Implementing a smaller focal length would be difficult. Increasing the lens size is possible but there are mechanical limits due to the extended water path. Imperium is currently working on a 3-in. lens design and is investigating the feasibility of a 5 in. lens. One problem with increasing the lens diameter is that the focal length must necessarily increase.

The most practical way to improve resolution is to increase the ultrasound frequency. Eq. 1 is linear, so doubling the frequency to 10 MHz would result in a halving of the resolution to 244 μm. Imperium proposes that increasing the frequency to 13 MHz poses no significant technical problem. The issue in increasing the ultrasound frequency is the increase in attenuation. The tradeoff between increased attenuation and improved resolution will be evaluated in the context of imaging breast tissue. Most conventional B-scan ultrasound systems operate at 12-13 MHz for imaging the human breast so the use of frequencies higher than 10 MHz is likely for the proposed system. Figure 6 shows an early image of mouse mammary gland obtained at 10MHz.

Ultrasound Field and Uniformity

As shown in Figure 14, we have already produced uniform wide-area fields. For a given field size, it has been found that the width of the active area of a pulsed source transducer must be approximately 50 % greater than the desired width of the ultrasound field used for imaging. Thus for a 2" field, a 3" wide transducer is required. The design challenge is the low impedance of such transducers. We used available PiezoCad software to design suitable impedance matching, and we have investigated commercial sources of high-energy pulsers in order to provide wide-field ultrasound with adequate pressure amplitude for imaging tissue in transmission. We plan to get the adequate source output energy to get a 3 inch square instantaneous field of view for our future medical imaging development.

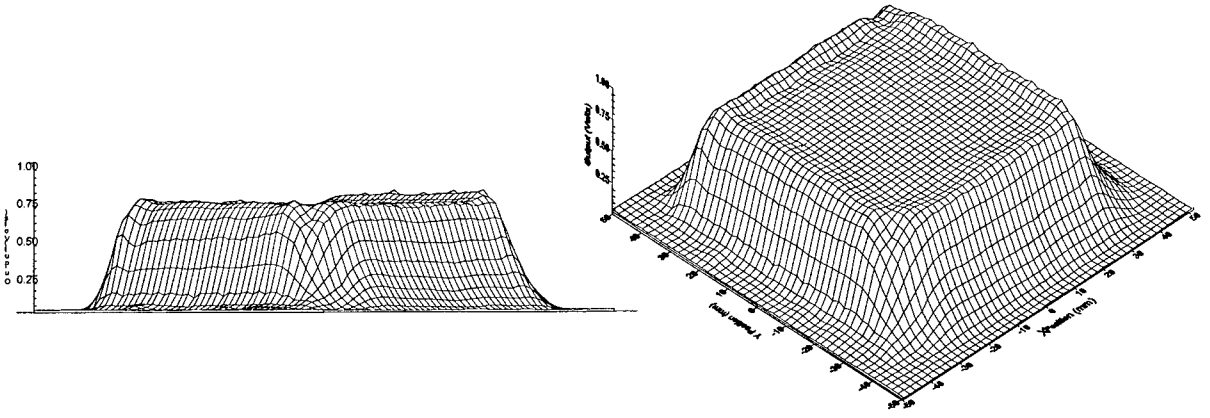

Figure 14: Uniform field from 1.5 MHz Stavely transducer pulsed by Metrotek MP270 pulser and Dapco calibrated hydrophone.

The far field of a transducer is given by the equation:

$$D_{FarField} = \frac{d^2}{4\lambda} \qquad \ldots (1)$$

where $D_{Far\ Field}$ = far field distance, d = transducer aperture, and λ = wavelength

For example, a 0.50 inch transducer operating at 5 MHz will have a wavelength of $\approx$ 0.012 inches in water, resulting in a far field of $\approx$ 5.21 inches. Thus all of the data collected with the proposed system will be done within the near field of the transducer.

Imperium engineers have calculated a number of measurements in order to characterize the performance of our transducers. Figure 2 shows a representative series of graphs that show the variation in pressure as a function of transducer aperture position for different distances away from the transducer. This data was collected for a 1.0-inch diameter, 5 MHz transducer. It was measured over a 30 × 30 mm aperture at distances from 0 to 150 mm from the transducer.

Note how the transducer pressure shown in a. is nearly uniform across the aperture with a sharp fall-off at the edges. As the distance from the transducer increases, the aperture shows a distinct lack of uniformity and the edge fall-off is not nearly as pronounced.

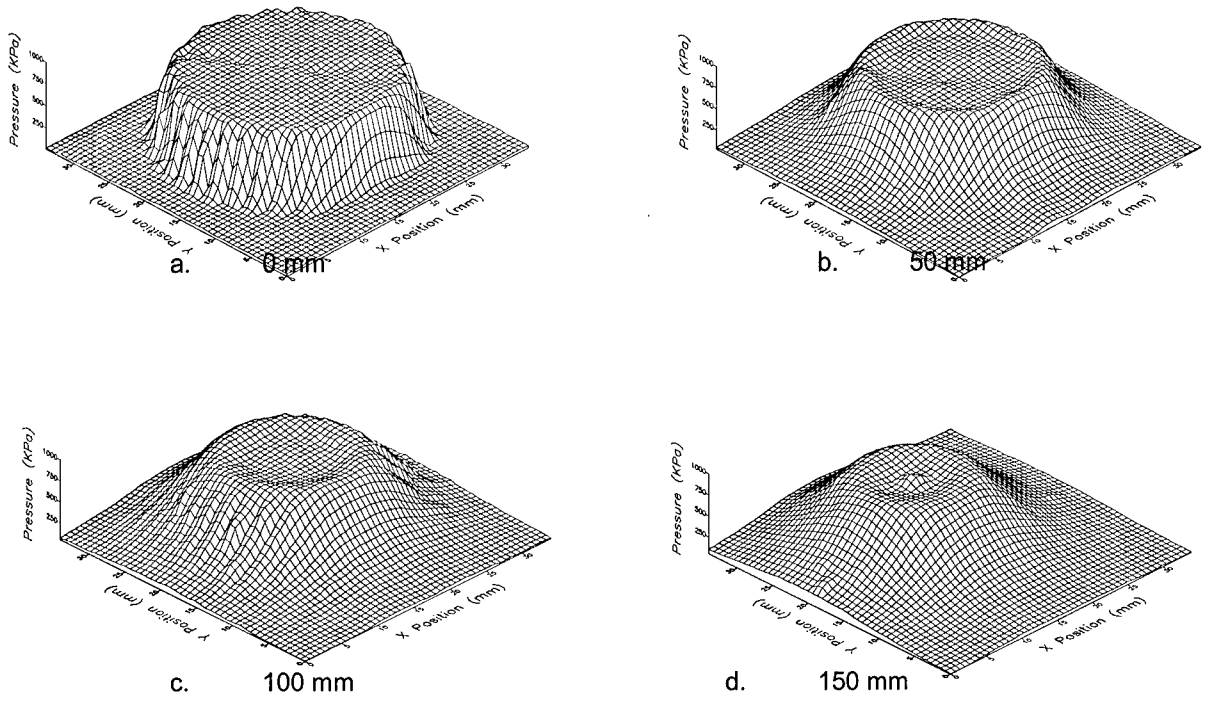

Figure 15 Transducer Pressure Variations with Distance

Zoom Lens Results

The ultrasound imaging system was set up and focused in a manner typically used for imaging with Imperium's ultrasound camera. The transducer was fixed in a position approximately 18 in. from the camera. The two lens elements are Imperium's two-element aspheric 2.75 in. diameter F/1 (Imperium 915 series) lens. Lens elements were moved relative to one another to achieve zoom. The change in image size and the lens positions were recorded. Image size was measured using the AcoustoVision Measurement™ tool (Imperium, Inc.).

Figure 16 shows the relationship of lens movement to image size. Note the monotonic change in image size versus lens change. This relationship is necessary to realize a practical zoom lens design.

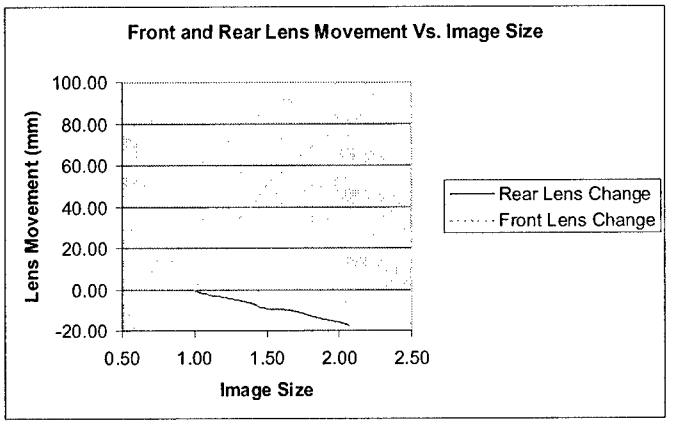

Figure 16 Lens Movement vs. Image Size

A 2:1 zoom was accomplished using a standard lens system by increasing the on-axis distance between the lenses. The front lens moved a distance of 80 mm and the rear lens moved 17 mm from the starting position. The images in Figure 17 show the reference image at the start and end points of the lens positions. Note the enlargement of the 1-in. marks on the ruler in Figure 17b.

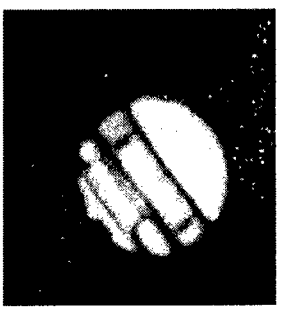

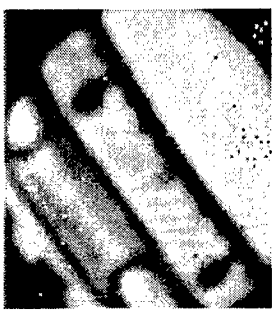

Figure 17a Image With no Magnification **Figure 17b** Magnified Image

Large (3") Field Of View

Two large area-imaging lenses were designed using the Zemax Optical Design Program (Focus Software Inc, Tucson, AZ). Both lens systems are composed of a large diameter objective lens and two smaller focusing elements. The lenses were designed to be diffraction-limited across the surface of the lens. Based on the design in Figure 18, the blur spot size at any given point in the image plane should be no greater than 375 μm for a lens with a three inch diameter, F/1 speed, and an ultrasound frequency of 5.0 MHz. Spot size estimates were performed for several points across the lens surface with the largest spot size occurring at the point farthest from the paraxial axis. The size of the plane wave to be focused and the size of the sensor array determine the magnification of the lens design. In this case, the lens focused a 76.2 mm diameter wave front onto a 10.8 mm square sensor array yielding a magnification of 0.14.

$$m = h' / h = 10.8 \text{ mm} / 76.2 \text{ mm} = 0.14. \quad \ldots (2)$$

m = magnification

h' = image height. h = object height

The first design consisted of two elements from the Imperium 915 lens with the addition of a third larger diameter objective lens. The working F-number of this design is 1.69 with an estimated off axis blur size of 375 μm. The Zemax Optical design program generated the ray tracing and spot size diagrams shown in Figure 18.

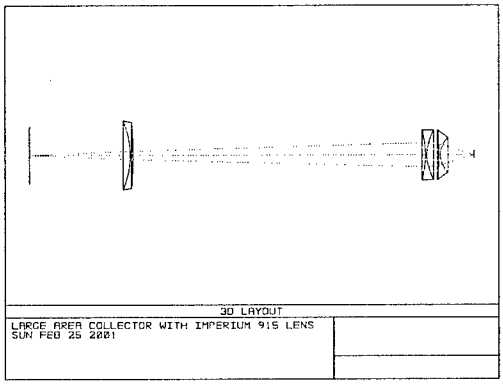

Figure 18a 3-in. Lens, Ray Tracing

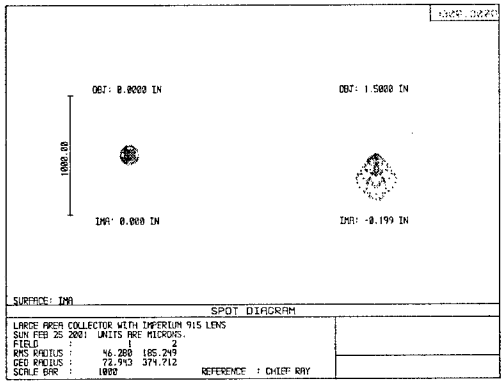

Figure 18b 3-in. Lens with 375 micron spot size

A second, improved design is similar but consists of three newly designed lens elements. The working F-number of this design is 1.68 with an estimated off axis blur size of 150 μm. Ray tracing and spot size diagrams of the second design are shown in Figure 19.

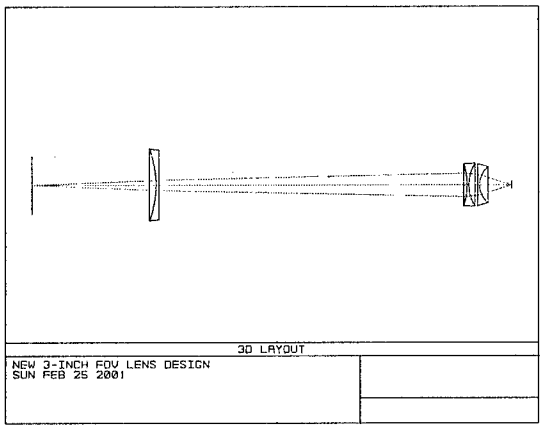

Figure 19a 3-in. Lens, Ray Tracing.

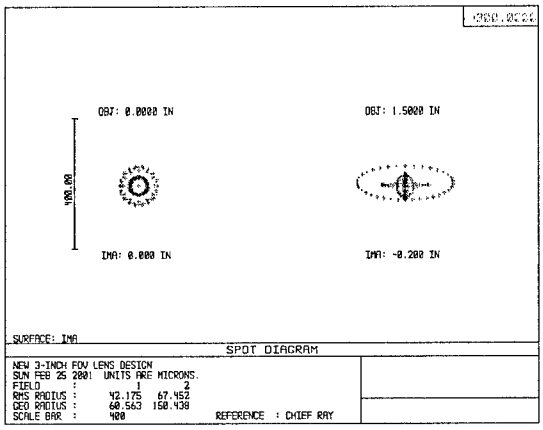

Figure 19b 3-in. Lens with 150 micron spot size

Improvements in Source Pulsers and Transducers

In order to meet our unique requirements for high-amplitude, wide-area ultrasonic fields, we have designed and built our own small, low-cost, high-voltage pulsers. The pulser design generates a 100 ns pulse with an amplitude variable from 0v to 1 Kv. We will increase the voltage amplitude to 2 Kv. Because of the low impedance of the required high-frequency, large-area source transducers, driving the transducers is difficult with a single pulser driver circuit. We are investigating the use of arrays of multiple smaller transducers each driven by a separate pulser circuit.

An interesting finding is that broadband composite transducers may be detrimental to this application. The lower attenuation at lower frequencies results in loss of spatial resolution. Narrowband ceramic transducers appear to produce a sharper picture. Figures 20a and 20b show the frequency responses of a ceramic and

composite transducers respectively. The peaks in Figure 20A are at 4.48 MHz and 5.78 MHz with attenuated low frequency response. The edges of the passband in Figure 20b are at 3.83 MHz and 6.96 MHz.

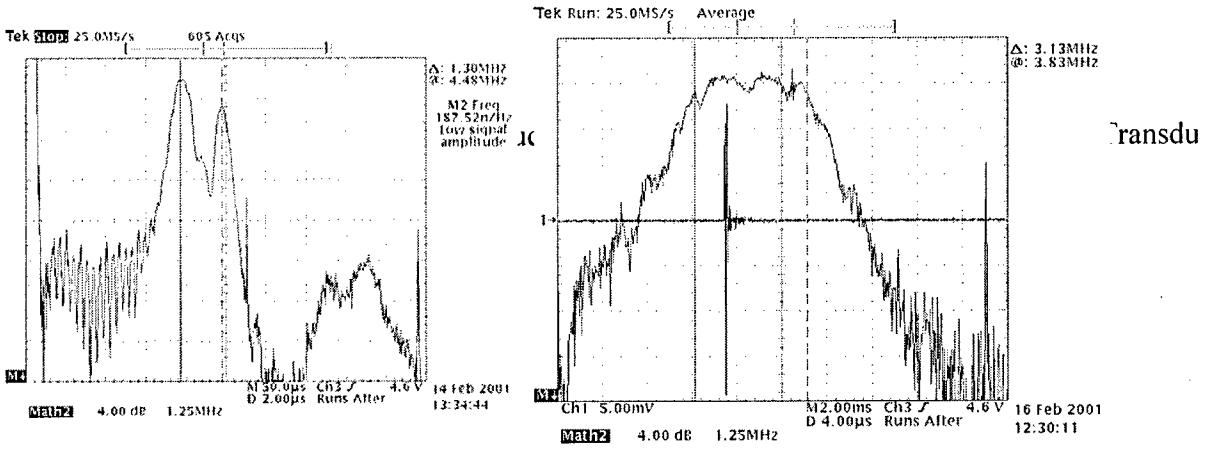

Figure 20: Frequency of a ceramic compared to a composite transducer.

Simulated Breast Biopsy

To prove the feasibility of using the proposed device in image guided needle biopsy we have performed imaging with a breast phantom. The images in Figures 21a and 21b were taken by Dr. Christopher Merritt of Thomas Jefferson University. The images are of a 1 cm fatty mass with needle embedded in a gelatin phantom. In Figure 21a notice the surface reflection at the bottom of the image, the reverberations from the needle, and the presence of speckle. These are common artifacts of pulse echo ultrasound. Figure 21b which was taken with the through transmission camera from Imperium clearly shows the needle and mass.

Figure 21a Pulse Echo Ultrasound Image
Needle in gelatin phantom

Figure 21b Transmission Ultrasound Image
Needle (white arrow) in phantom next to 1cm mass.

A second set of images (Figure 22) was taken with a CIRS phantom at the Georgetown University Medical Center. Figure 22 shows the sequence of needle biopsy images. The images were sampled from a sequence of 150 ultrasound images taken from 30 frames per second for five seconds. The Imperium ultrasound camera was focused on two small, simulated masses and a biopsy needle about 4 cm below the surface. The needle first punctured the target (a) and (b), then left (c), and punctured the target again (d) and (e). The needle was rotated clockwise from (e) to (f). This operation pushed the mass on the right upper corner out of the focal plane.

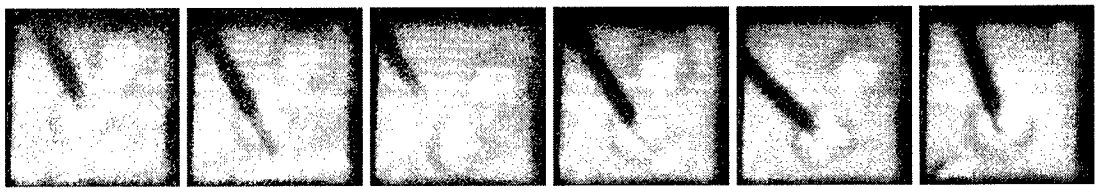

(a) (b) (c) (d) (e) (f)

Figure 22. Needle Biopsy Sequence

In summary, we found the prototype system based on this hybrid microelectronic array that is capable of generating ultrasound images with fluoroscopy-like presentation and without speckle artifacts. The images show no obvious geometrical distortion. The resolution study indicates that a spatial resolution at ~320 microns was observable using a fan-line phantom and calcification phantom. The contrast resolution study indicates that the system is capable of differentiating objects 3mm in size with low differential contrast. The difference between the target and background materials in this experiment was as low as 0.07 dB/cm/MHz.

The potential for use in biopsy procedures is demonstrated through the imaging of breast phantoms with simulated tumors. The system is capable of imaging the area of interest in real-time.

Images of human breast tissue

With delivery of the newest research system, we started to image human breast tissue removed at surgery. The images show details within the tissue, but these images are complicated because there still air in these surgically removed tissue and air prevents the transmission of the ultrasound. The specimens we have used contain fatty and fibrous tissue. There are small areas of glandular tissue and sometimes skin included in the specimens. Examples are given on the next few pages.

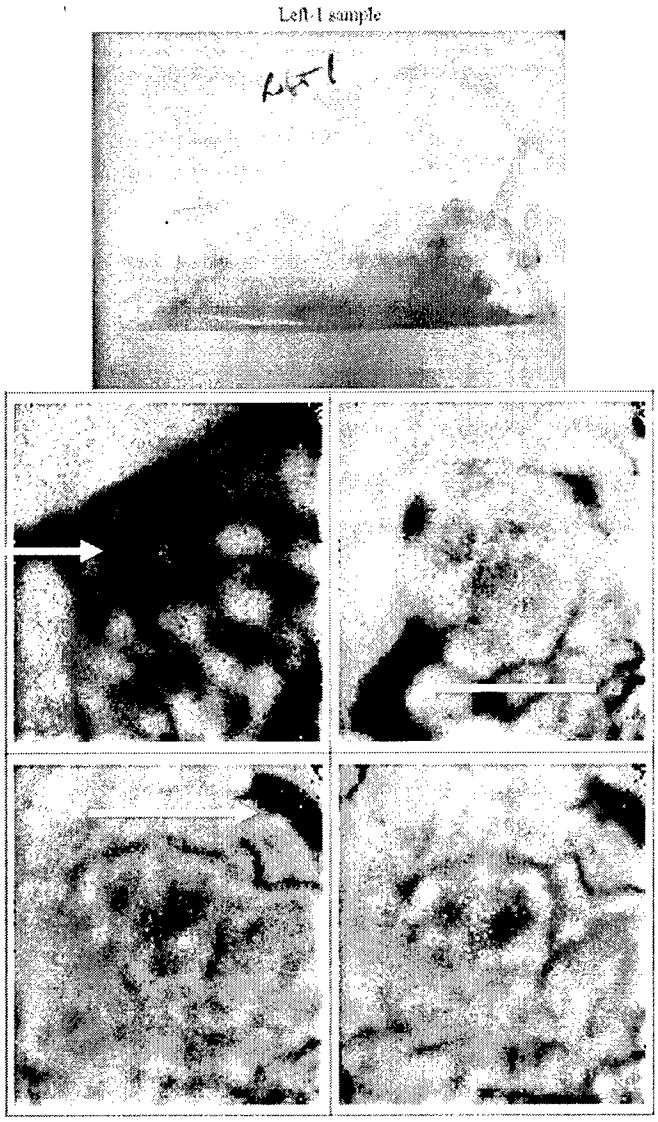

Figure 23: These images are through areas of fatty breast tissue. The black areas represent air pockets (white arrows).

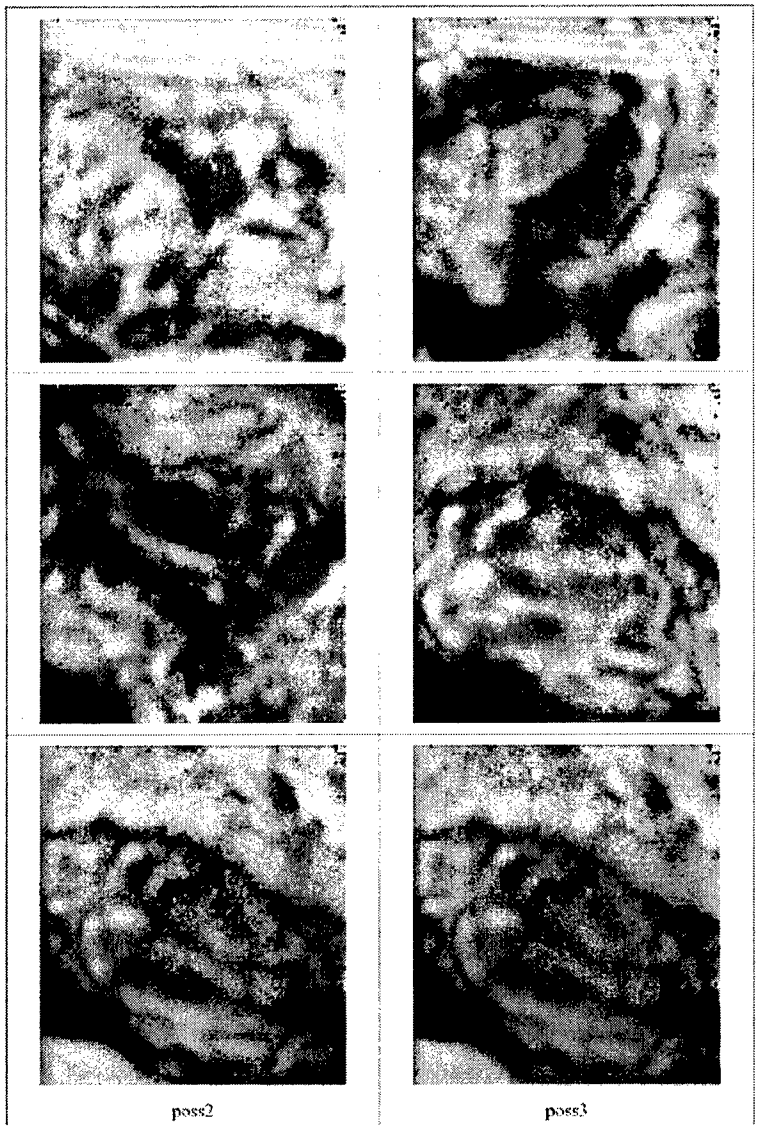

Figure 24: This is a series of images through fatty breast tissue. It shows the lobulation of fat that we see with this ultrasound system.

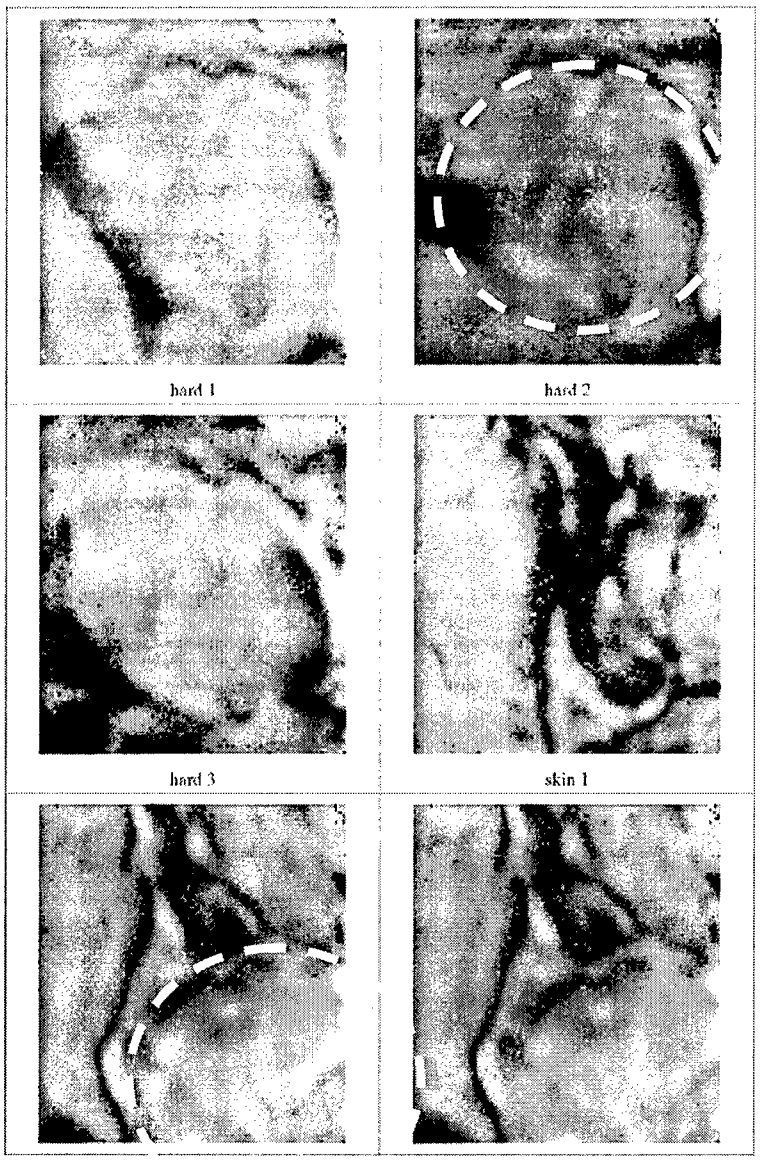

Figure 25: This is a series of images through a focal area of fibrous tissue. The dotted white circles outline the area of fibrous tissue on two images that can be compared to their neighbors without the dotted white circles.

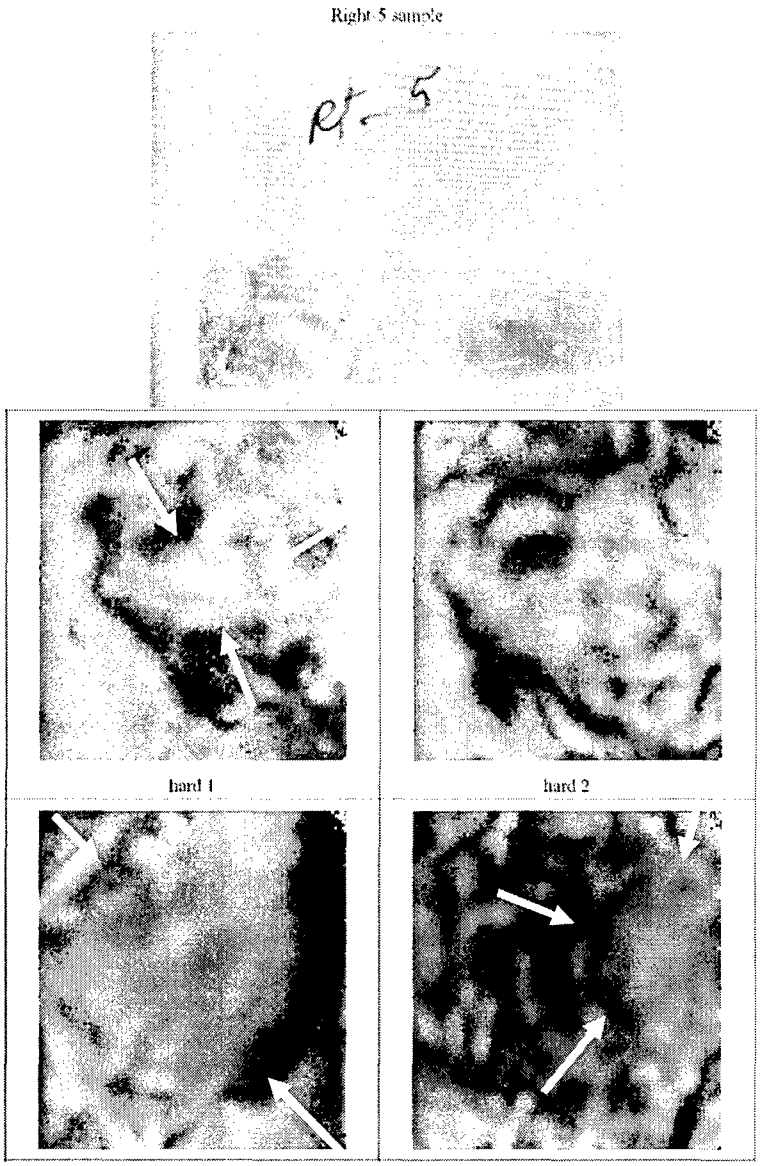

Figure 26. Two separate areas of fibrous tissue, one large and one small, surrounded by fat. (White arrows point to the two fibrous tissue areas.)

Dry System Implementation

A dry system (no water tank) is required as a practical approach to implementation of a through transmission ultrasound system for medical applications. Imperium has therefore designed and constructed two proof of concept systems for in vivo imaging. For the first, the ultrasound camera and source transducer were placed on opposing ends of a C-arm mount. The patient would be placed between the camera and source for imaging. A picture of the prototype dry system is shown in Figure 27.

The C-arm system is designed to provide a means of dry-coupling a patient to an Imperium ultrasound camera in the through-transmission configuration. The system has several degrees of freedom to allow it to move into a convenient position for patient coupling. There are flexible acoustic coupling pads on the transducer and camera sides of the device to provide a comfortable, conformable interface with a variety of irregularly shaped objects. The entire C-arm is mounted to a wheeled cart for added mobility. User interface is accomplished with a standard monitor, keyboard and mouse, along with typical pulser controls.

In testing this system with breast phantoms, it became immediately apparent that when ultrasound coupling gel is used, the system does not adequately fix the breast in place and that the phantom, and therefore a breast, would slide out of the device. Thus modifications of this C-arm system are underway to provide a broader platform to support the breast. The design of this c-arm device is similar to initial systems developed for preclinical testing of digital mammography—designed for spot imaging of the breast since larger solid state digital detectors were not then available.

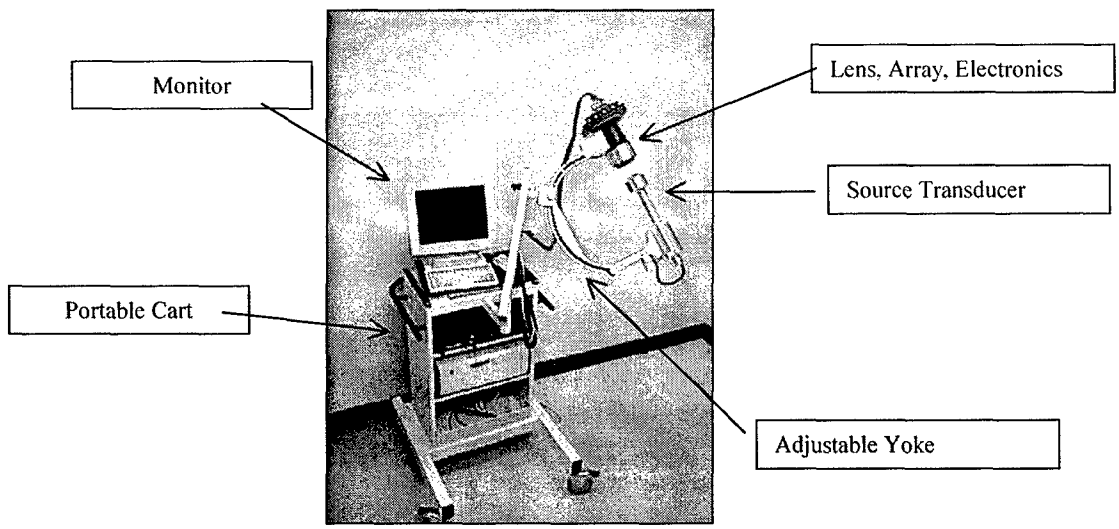

Figure 27 Proof of Concept C-arm System

The second prototype version for in vivo imaging of the breast.

A second prototype system is currently almost ready for testing. It provides a firmer method for support of the breast during imaging by providing a flat support panel that goes both below and above the breast and uses light compression to flatten the breast. A stepping mechanism has been designed so that the imaging components can be moved in steps across the breast so that the entire breast can be imaged. The system is almost ready for delivery to Georgetown for testing, but the stepping motor has not yet been installed and the stitching software to "stitch" together the separate image frames is not yet complete. The current prototype will currently allow only crainocaudal (CC) views, but this system will allow us to test many components of the imaging system and its software and will help us design the next iteration of the in vivo imaging system.

Figures 28 and 29 show the prototype ultrasound breast imaging system that was built by Imperium, Inc. This device mimics the operation of a standard mammogram machine in the fact that the patient's breast is slightly compressed between two plates and an ultrasound beam is then passed through the breast and imaged by the Imperium camera to create an x-ray –like, plan view image. The system can be adjusted to accommodate patients of different heights and breast thicknesses.

The camera can not image the entire breast at one time since the field of view of the camera is limited to a 1" x 1" area. Therefore, both the camera and transducer are to be scanned over the region of the breast and the 1" images would then be "stitched" together to form one large image of the breast. "Stitching" was also used in some early digital mammography systems including an early version of the Lorad system.

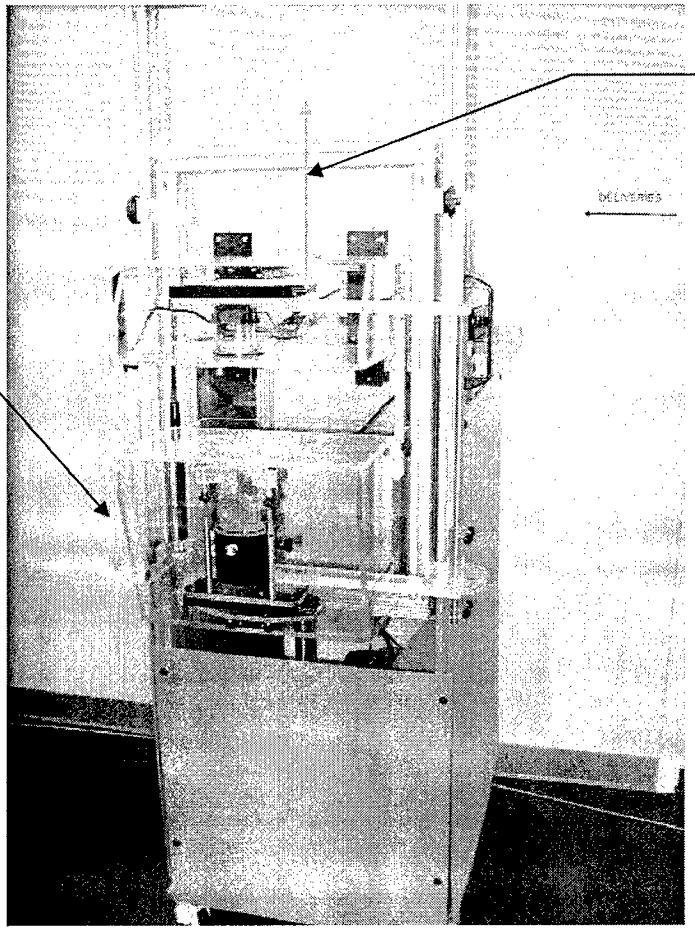

Figure 28. Prototype Ultrasound Breast Imaging System

Figure 29 shows the detail of the measurement area of the system. A transducer is positioned above the patient's breast, while the camera is below. Both devices slide on the plastic plates that are used for light breast compression. A handle on the right-hand side, allows the operator to move both the transducer and the camera together as a single unit so that the transducer is always "looking" directly into the camera. The operator uses the handle to manually move the measurement system over the region of interest.

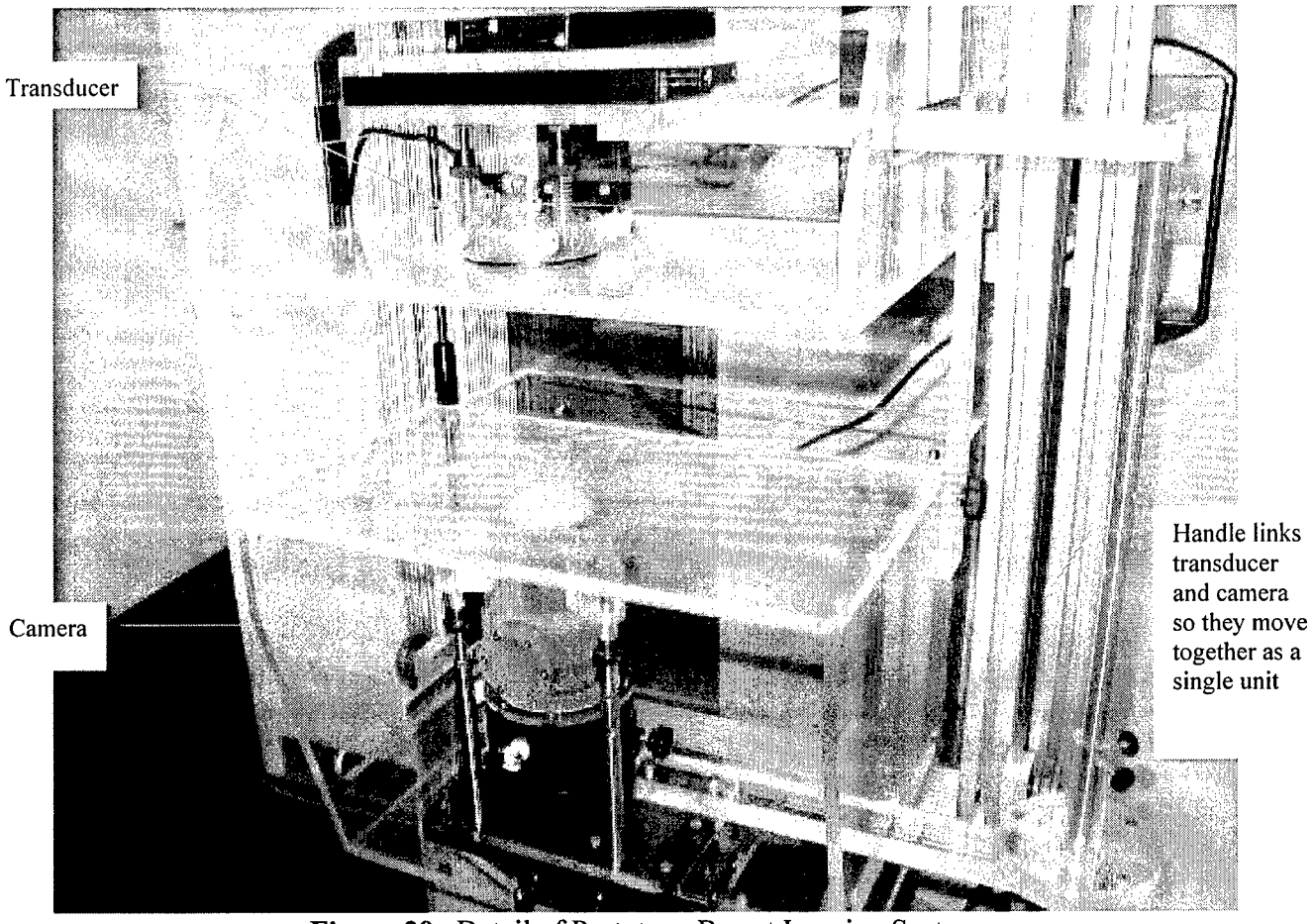

Figure 29. Detail of Prototype Breast Imaging System

Future versions of this device could replace this manual movement by one where a computer controls a stepper motor system that drives the system over a designated region of interest. Imperium has constructed a prototype of such a system that is shown in Figure 30.

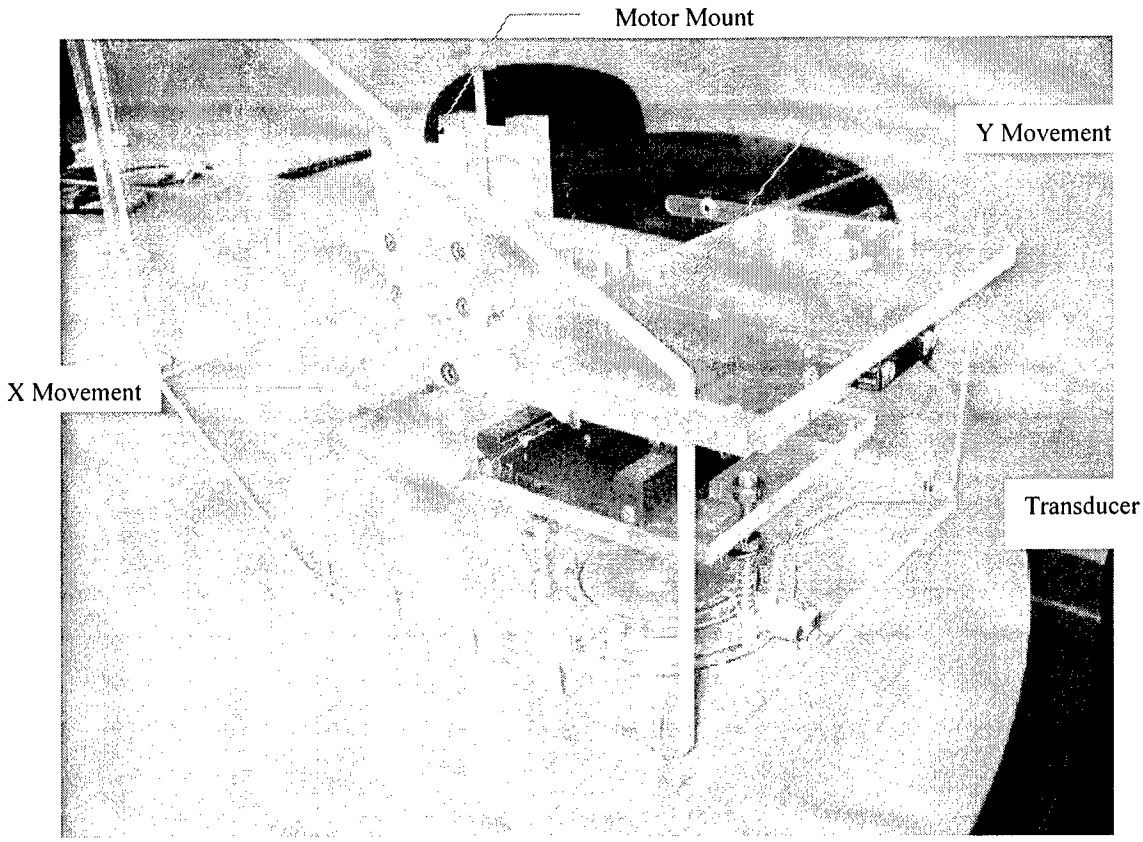

Figure 30. Prototype Motor Driven Transducer Stage

The single stage shown in Figure 30 allows stepper motors to be mounted and to drive the transducer in both the X and Y directions. Only a single motor mount is shown in Figure 30 (with no motor present). The motor moves the transducer through a rack and pinion drive system shown in Figure 31.

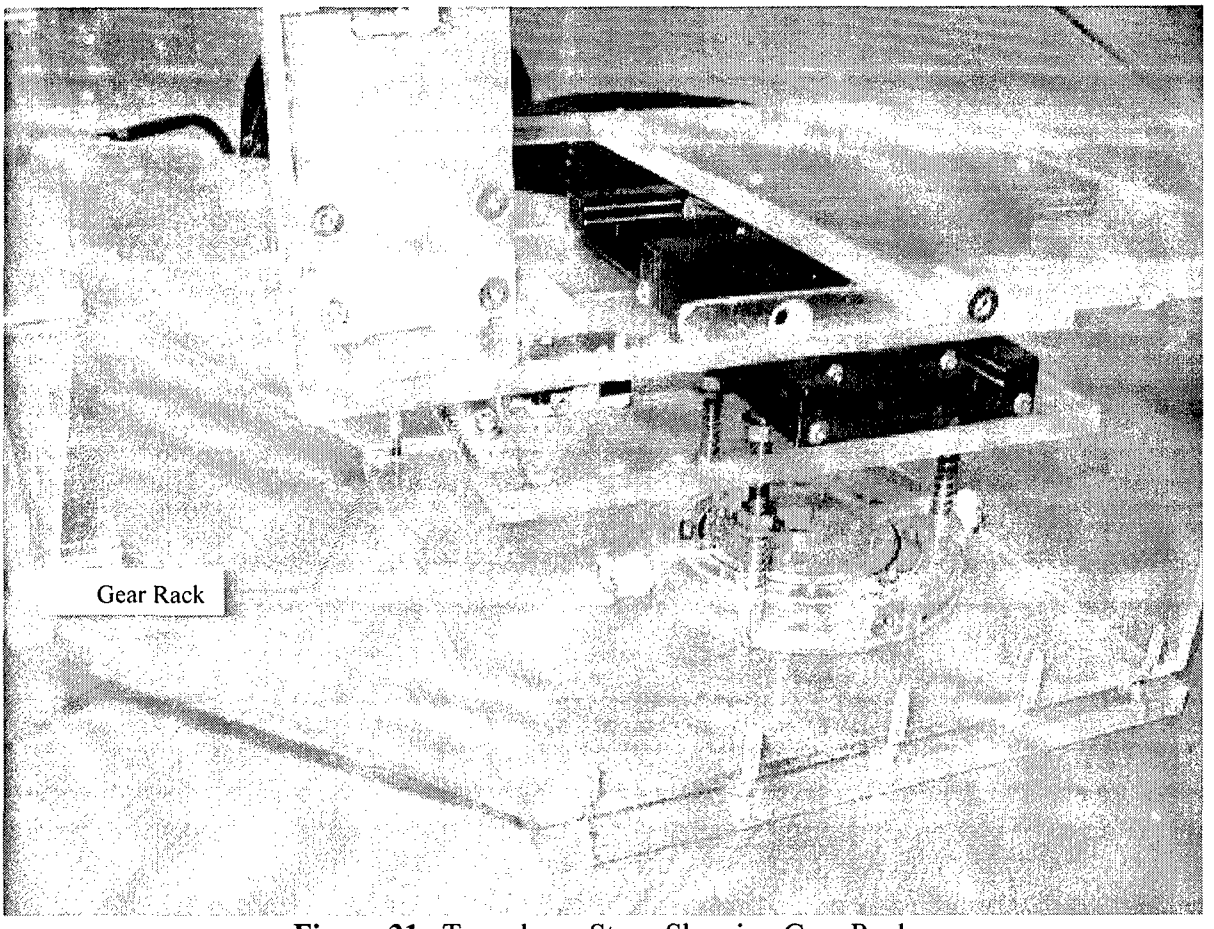

Figure 31. Transducer Stage Showing Gear Rack

By making this type of stage for both the transducer and the camera, the operator will be able to move the system under computer control and to better define the measurement areas where the plan view ultrasound images are being collected. By knowing the X and Y coordinates (through stepper motor feedback), it will also be easier to stitch together the individual 1" x 1" images into a composite image.

Key Research Accomplishments

We continue to improve our understanding of the parameters of this novel transmission ultrasound system and continue to work with Imperium, Inc on improvements. Improvements have been made in the resolution of the system and in its dynamic range as demonstrated above. We have just started to image human breast tissue specimens and are about to place the research unit in the clinical breast imaging center so that we will be able to compare biopsy specimens on both the experimental transmission system in comparison to conventional reflection ultrasound. The second prototype for in vivo breast imaging is almost ready to be delivered to us. Using the data from this project as preliminary data, we submitted a proposal to NIH and have recently received two years of funding from The National Institute for Biomedical Imaging and Bioengineering (NIBIB) to continue development of the system and for a small in vivo clinical trial.

Reportable Outcomes: Publications

Copies of these publications are included in the appendix.

Lo S-C.B, Rich D, Lasser ME, Kula J, Zhao H, Lasser R, and Freedman MT, "A C-Scan Transmission Ultrasound Based on a Hybrid Microelectronic Sensor Array and Its Physical Performance," SPIE Proc. Med. Img. Vol. 4325, pp. 89-95, 2001.

Liu CC, Lo S-C. B., Freedman M.T., Rich D., Kula J., Lasser R., Lasser M.E., Zeng J., Ro D., "Projection Ultrasound and Ultrasound CT using A PE-CMOS Sensor: A Preliminary Study," Proceedings of the SPIE Medical Imaging Conference, Vol. 5373, pp. 61-69, 2004.

Lo S-C.B, Liu C, Freedman MT, Kula J., Lasser R., Lasser M., and Wang Y., "Transmission and Reflective Ultrasound Images using PE-CMOS Sensor Array," SPIE Proc. Med. Img. Vol. 5750, pp. 69-78, 2005.

Other

One of our graduate students, Chu-Chuan Liu received a Pre-Doctoral Fellowship Award (# DAMD17-01-0197) from the US Army Breast Cancer Program to perform his research on the technical aspects of the Imperium Transmission Ultrasound System. He presented a poster on this at the US Army Breast Cancer Era of Hope Conference in Orlando, FL, Sept 25-28, 2002. A copy of the poster is included in the appendix.

Statement of work with approved modifications

During the course of this project, the original statement of work was modified (with approval) several times. Modification was necessary because the US Army Congressional Directed Program allocated moderately less funding that originally requested; we encountered unexpected complexity of the engineering for the new device in delays in the delivery of systems to Georgetown; we encountered difficulty in obtaining approval from both the US Army Human Subjects reviewers and the Georgetown Institutional Review Board for the same research protocol and consent forms. Substantial work has been accomplished, but by the nature of this project, work is continuing, rather than completed. Because additional funding has been received from NIH-NIBIB, additional development will continue.

Imperium's tasks

- *System modifications and adjustment* ..... *.Months 1 –**Initial work complete; new work continuing***
- *Training GU technical members* .....*Month 5 - **Initial work complete; new work continuing***
- *Assist in physical evaluation* .....*Month 5 - **Initial work complete; new work continuing***
- *Development of modified system based on information learned to this point.*
- *Building of new prototype* *Months 2-15 - **Initial work complete; new work continuing***
    - *New transducer design complete*

- *Machine design: complete*
- *Manufacturing started*

• *Training GU clinical members* ..... *Month 9 - **Initial work complete; new work continuing***

• *Assist in pre-clinical testing* ..... *Month 10-18 - **Initial work complete; new work continuing***

• *System maintainance and upgrade* ..... *Month 5-24 –**Laboratory system replaced.***

Tasks assigned to Georgetown

- *Performance evaluation of the laboratory system* ..... *Months 5- 9* ***Complete***
- *Deblurring methods to improve visualization of masses (phantom study)* .....*Months 10 – 12* ***Complete***
- *Image enhancement study to signals of calcifications (phantom study)* .....*Months 11 – 14* ***Complete***
- *Recommendations to Imperium on modification of the device* ***Initial work complete; new work continuing***
- *Assistance in design of new prototype* ***Initial work complete; new work continuing***
- *Evaluation of system using animal tissues* ***Complete***
- *Evaluation using human breast tissue: biopsy specimens, partial mastectomies, and mastectomies, if available.* ***Ongoing.***

Conclusions

Over the years of this project, progress was slower than expected because of the complexity of engineering problems encountered. We had initially received moderately less than our originally requested amount of funding. We encountered problems in obtaining concurrent approval from the US Army Human Subjects Reviewers and the Georgetown Institutional Review Board. We have seen significant improvement in the design and operating characteristics of the Imperium C-Scan Transmission Ultrasound system and have started to test the latest prototype on human breast tissue. We have received additional funding from The National Institute for Biomedical Imaging and Bioengineering (NIBIB) to continue development of the system and for a small in vivo clinical trial. We have approval from the Director of Breast Imaging at Georgetown to place the research unit in the clinical breast imaging facility and are about to start dual imaging of biopsy specimens with the research transmission ultrasound system and a high quality conventional system so that the imaging patterns can be more accurately compared. A system for in vivo human breast imaging is close to ready for delivery to Georgetown for early clinical evaluation.

References:

[1] McDicken WN, "Diagnostic Ultrasonics" Third Edition, Churchhill Livingstone, 1991

[2] Ishisaka A, Ohara H, and Honda C, " A New Method of Analysis Edge Effect in Phase Contrast imaging with Incoherent X-rays," Optical Review, Vol. 7, No. 6, pp.566-572, 2000.

[3] Freedman MT, Lo S-C.B, Honda C, Makariou E, Sisney G, Pien E, Ohara H, Ishisaka A, Shimada F. "Phase contrast digital mammography using molybdenum x-ray: clinical implications in detectability

improvement". Proc. SPIE Vol. 5030, p. 533-540, Medical Imaging 2003: Physics of Medical Imaging; Martin J. Yaffe, Larry E. Antonuk; Eds.

A C-Scan Transmission Ultrasound Based on a Hybrid Microelectronic Sensor Array and Its Physical Performance

Shih-Chung B. Lo[*,a], David Rich[b], Marvin E. Lasser[**,b], John Kula[b], Hui Zhao[a], Bob Lasser[b], and Matthew T. Freedman[a]

[a]ISIS Center, Department of Radiology, Georgetown University Medical Center, Washington, D.C.
[b]Imperium Inc. Rockville, MD

ABSTRACT

A C-scan through-transmission ultrasound system has been constructed based on a patented hybrid microelectronic array that is capable of generating ultrasound images with fluoroscopic presentation. To generate real-time images, ultrasound is introduced into the object under study with a large unfocused plane wave source. The resultant pressure wave strikes the object and is attenuated and scattered. The device detects scattered as well as attenuated ultrasound energy which allows the use of an acoustic lens to focus on detected energy from an object plane. The acoustic lens collects the transmitted energy and focuses it onto the ultrasound sensitive array. The array is made up of two components, a silicon detector/readout array and a piezoelectric material that is deposited onto the array through semiconductor processing. The array is 1 cm on a side consisting of 128×128 pixel elements with 85μm pixel spacing. The energy that strikes the piezoelectric material is converted to an analog voltage that is digitized and processed by low cost commercial video electronics. The images generated by the device appear with no speckle artifact with fluoroscopy-like presentation. The images show no obvious geometrical distortion. The experimental results indicated that the system has a spatial resolution of 0.32 mm. It can resolve 3mm objects with low differential contrast and an attenuation coefficient difference less than 0.07 dB/cm/MHz. Phase contrast of the objects are also clearly measurable. A presentation of a C-scan image guided breast biopsy was demonstrated. In addition, punctured needle tracks in a tumor was clearly observed. This implies the potential of observing the spiculation of masses in vivo.

Keywords: Ultrasound sensor array, breast imaging, ultrasound, and transmission ultrasound.

1. INTRODUCTION

A variety of medical imaging modalities are presently available for diagnosis of soft tissues. Clinically, X-ray radiography and ultrasound imaging serve as first line examination tools. MRI has strong tissue characterization capability with outstanding resolution. SPECT and PET both produce relative low resolution and noisy images; they can be used to study the physiology of the organ and to examine possible abnormality associated with the chemical up-take of the tissue. In addition, both MRI and SPECT are used to perform advanced diagnosis and/or staging the disease when necessary. Many potential clinical research applications using MRI and SPECT are still under investigation.

Mammography is the most successful soft x-ray modality that is used for examining breast abnormalities[1,2,3,4]. However, it has several limitations[5,6]. For example (a) it is insensitive to dense breasts, (b) it has a two-dimensional projection image that obscures the breast structures and abnormalities, (c) its continuous x-ray exposure is not recommended, (d) it has a relatively high false-positive which increases the cost in unnecessary work-up, biopsy, and patient anxiety, and (e) it causes unpleasant compression of breasts during x-ray procedures.

Clinical interpretation of conventional ultrasound images can be very complex resulting from general acoustic heterogeneity of the organ and similarity in acoustic properties between normal and abnormal tissues. Depending upon ultrasound frequency, the resolution of the current ultrasound imaging is approximately 1-2 mm at a depth of 2-3 cm and about 5-7 mm at a depth of 5-6 cm [Sigel 1995]. These two major problems hinder the current ultrasound as an effective diagnostic tool for both breast cancer[7,8] and prostate cancer[9,10,11] diagnoses. Clinically, ultrasound has been used in assessing dense breast regions and in distinguishing between cysts and solid masses[12,13,14].

By merging knowledge gained in the advanced acoustic science and sensor technology, we have implemented a novel research system that produces real-time speckle-free images of human soft tissues. In this paper, we introduce this potential new medical ultrasound system based on a newly invented ultrasound sensor chips. This high-resolution distortion-free ultrasound imaging system has unique potential for improved soft tissue diagnosis in general. We have also conducted a series of physical evaluation studies to investigate the performance of this prototype system and its clinical potential.

2. MATERIAL AND METHODS

2.1. The C-Scan Prototype System Configuration

The basis for the proposed device is a novel patented two-dimensional imaging system that creates immediate, high-resolution images of subsurface structures. Imperium has developed and patented a hybrid microelectronic array that is capable of generating a real time area scan of images at 30 frames per second or higher.

To generate real-time images, ultrasound is introduced into the target under study with a large unfocused ultrasound plane wave. The resultant pressure wave strikes the target and is attenuated and scattered. An acoustic lens collects the energy and focuses it onto the ultrasound sensitive array. The array is made up of two components, a silicon detector/readout array and a piezoelectric material that is deposited onto the array through semiconductor processing (see Figure 1). The array is 1 cm on a side consisting of 128×128 pixel elements (16,384) with 85μm pixel spacing. The energy that strikes the piezoelectric material is converted to an analog voltage that is digitized and processed by low cost commercial video electronics.

Note that there is an ultrasound receiving (piezoelectric) layer deposited onto the chip. A completed array is shown in Figure 2. The array is responsive over a wide range of ultrasound frequencies, although most imaging is done between 1MHz and 10MHz. The use of a lens provides a simple, inexpensive alternative to complex beam forming often employed in ultrasound imaging. The user simply focuses by adjusting the lens while looking at the image on a monitor. Furthermore, it provides a means to trade off resolution and area coverage, or zoom in and out.

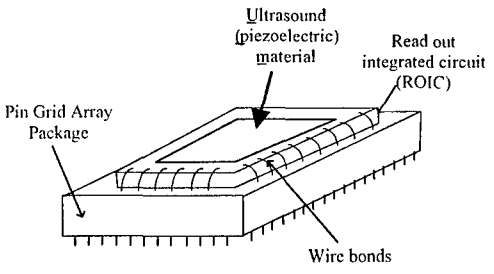

Figure 1: Schematic of array

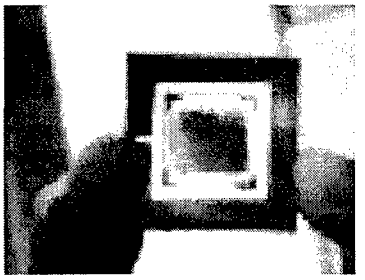

Figure 2. 128 × 128 assembled array

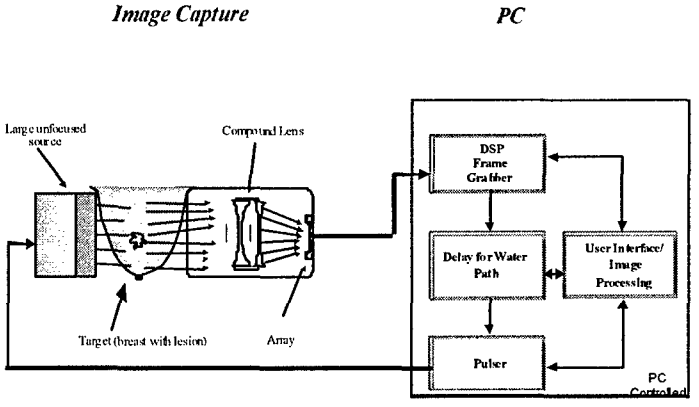

Figure 3. The prototype system configuration

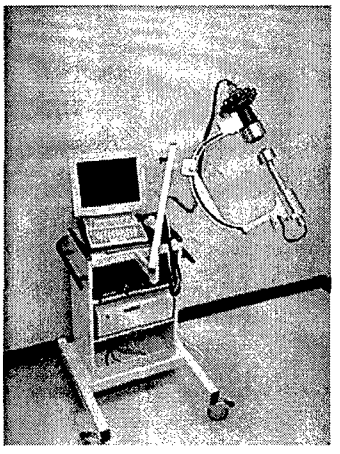

Figure 4. A C-scan system under construction

The system operates by pulsing a commercial off-the-shelf ultrasonic spike pulser. This excites the large area unfocused ultrasound transducer (only used as a source) and sends an ultrasound plane wave through the water. This plane wave enters the target, scatters, exits the target and strikes the acoustic lens which collects the scattered energy and focuses it onto the array. This operation repeats 30 times/second. Standard video electronics and image processing are used to format the image for presentation to the user and perform real time image processing; either on a PC monitor or hand held LCD. To remain compatible with standard RS-170 video equipment, the imagery is typically presented at 30 frames/second. Higher frame rates are available if needed. Figure 3 schematically shows this architecture for the inspection of an object. Figure 4 is a furnished system for clinical evaluation. The sensor array and the ultrasound source are located in the top and bottom compartments of the C-arm, respectively.

2.2. Evaluation of System Performance

The evaluation study was performed in a fixed water tank environment. The ultrasound was operated at peak frequency of 5MHz using a broad band unfocused planar wave (1.5" square) transducer (Krautkramer Model No. 389-040-550 S/N 00LMW5). The pulser was a SDI/Imperium I-100 standard pulser S/N – 001. The hydrophone was a provided by Specialty Engineering (Model GL-0400, SN G727). Time and frequency plots of the ultrasound wavefront are shown in figure 5. The hydrophone has a sensitivity of 22.4KPa/mv at 5MHz. Figure 5b shows a peak-to-peak amplitude of 34mv with a resulting sound pressure level is 762KPa. Figure 5a shows a peak frequency response at 4.48MHz and 5.78MHz with a low frequency rolloff.

The acoustic lens used was a two-element aspheric 50mm diameter F/1 (Imperium 914 series). The camera contains an Imperium proprietary sensor array (Model I-110 S/N 013 Array S/N 17-8). In order to acquire the signal in real-time, the circuit signals were converted to video signals and digitally recaptured at 8-bit per pixel by a frame grabber at 1/30 second. An on the shelf frame grabber (Matrox Meteor II standard) was adapted in the system. For display purposes, the pixels were interpolated in the camera to produce a 440 × 440 pixel display. We have conducted a series of studies for the evaluation of system performance using the prototype system described in this paper. These studies were performed using phantoms made by CIRS (Computerized Imaging Reference Systems, Inc., Norfolk, VA). Since conventional ultrasound phantoms do not meet the requirements of C-scan through-transmission imaging systems, we designed the three phantoms specifically for this study including (1) small sphere phantoms to simulated nodules in breast mimic background, (2) a fan of seven wires for measuring resolution, and (3) simulated microcalcifications in breast mimic background. Additionally, a standard CIRS breast phantom containing simulated cysts and tumors for biopsy simulations was also used in the study.

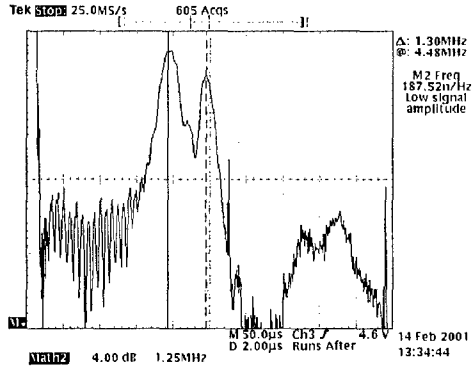

Figure 5A. Transducer Frequency Response

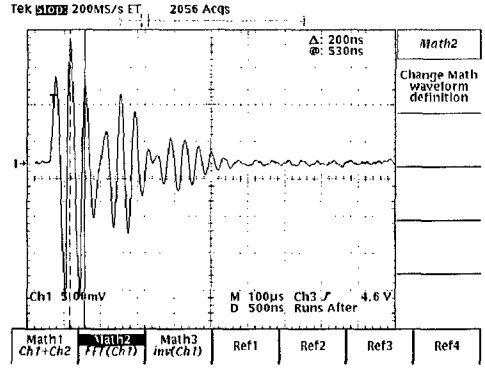

Figure 5B. Time Domain Response

3. Experiments and Results

3.1. Evaluation of Contrast Resolution

Two sets of spheres were inserted in a background material (Zerdium™) the density of which is designed to simulate breast tissue. The density of the background material is 0.22 dB/cm/MHz. Each set consists of four spheres with different ultrasound attenuation: 0.06, 0.15, 0.5, and 0.8 dB/cm/MHz. The first set of spheres are 3mm in size and the second set of spheres are 5mm. Figure 5 shows the images of the 5mm spheres taken with the prototype system. The field of view of the prototype system is limited so two pictures were taken for this set of spheres. Figure 6 shows the images of the 3mm spheres. We also performed a quantitative measure using contrast-to-noise-ratios (CNR) for each sphere. The CNR was computed as follows:

$$CNR = (f_m - b_m)/\sqrt{(\sigma_f^2 + \sigma_b^2)/2}$$

where f_m and b_m are mean intensity values of foreground and background, repectively. σ_f and σ_b are the corresponding standard deviations. Tables I and II list the results of CNRs for 5mm and 3mm spheres, respectively. In Figures 6 and 7, the edges of the cyst mimicking and tumor mimicking spheres are clearly observed with a phase contrast phenomenon. The phase contrast is fundamentally due to the ultrasound refraction and refers to multiphased wavefront in which individual phases of the wave arrive at the sensor possessing 180° out of phase that cancel a significant part of wave amplitude or 360° in-phase that add the amplitude. When the refraction index of the object is greater than the background, the refraction beams are angled outward. When the refraction index of the object is greater than the background, the refraction beams are angled inward. Recently, an outward refraction phase contrast phenomenon was discovered in incoherent x-rays by Ishisaka, et al using a projection geometry[15]. However, x-rays cannot produce an observable in-phase contrast at this point of technology development.

(A) Images of 2 simulated cysts (5mm) (B) Images of 2 simulated tumors (5mm)

Figure 6. The C-Scan images of the four 5mm spheres using Zerdine™ background at 0.22 dB/cm/MHz. (A) Cysts mimicking spheres with 0.06 dB/cm/MHz at the left and 0.15 dB/cm/MHz at the right. (B) Tumor mimicking spheres with 0.5 dB/cm/MHz at the left and 0.8 dB/cm/MHz at the right.

Table I. CNRs of the four 5mm spheres imbedded in a Zerdine™ background at 0.22 dB/cm/MHz.

Sphere in dB/cm/MHz	0.06	0.15	0.5	0.8
Mimicking structures	Cyst	Cyst	Tumor	Tumor
CNR	4.88	1.85	-2.27	-5.70

(A) Images of 2 simulated cysts (3mm) (B) Images of 2 simulated tumors (3mm)

Figure 7. The C-Scan images of the four 3mm spheres using Zerdine™ background at 0.22 dB/cm/MHz . (A) Cysts mimicking spheres with 0.06 dB/cm/MHz at the left and 0.15 dB/cm/MHz at the right. (B) Tumor mimicking spheres with 0.5 dB/cm/MHz at the left and 0.8 d B/cm/MHz at the right.

Table II. CNRs of the four 3mm spheres imbedded in a Zerdine™ background at 0.22 dB/cm/MHz.

Sphere in dB/cm/MHz	0.06	0.15	0.5	0.8
Mimicking structures	Cyst	Cyst	Tumor	Tumor
CNR	3.49	1.97	-3.40	-3.62

3.2. Evaluation of Spatial Resolution

We designed a line-bar phantom in such way that seven stainless steel wires at 250 microns were arranged with a fan pattern as shown in Figure 8 (A). Figure 8(B) is the images of this phantom. Figure 8(C) shows the inversed intensity profile at the level of two black arrows shown in (B).

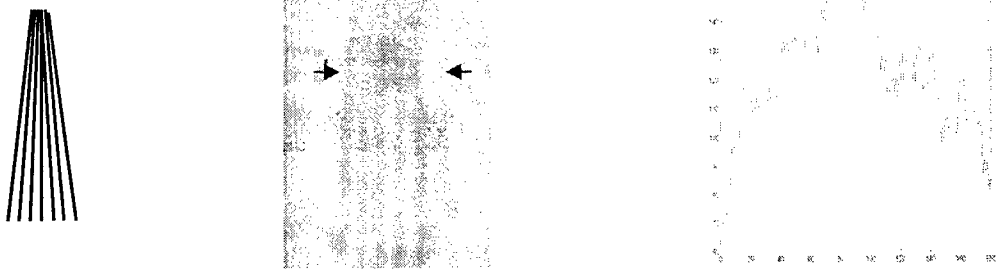

(A) (B) (C)

Figure 8. A fan-lines phantom is shown in (A), image of the fan-lines in (B), the inversed intensity profile in (C) at 0.32 mm spacing at the level indicated by the two black arrows in (B).

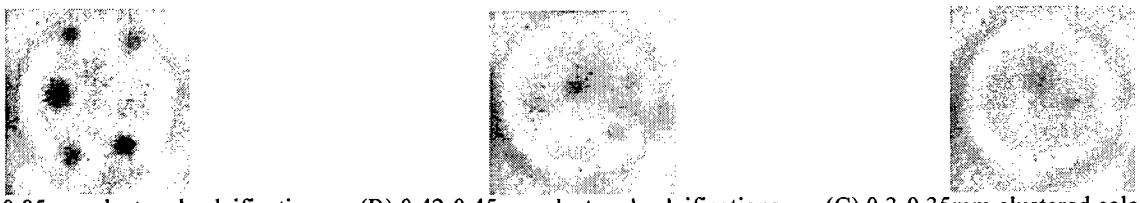

(A) 0.7-0.85mm clustered calcifications (B) 0.42-0.45mm clustered calcifications (C) 0.3-0.35mm clustered calcifications

Figure 9. Images of the C-scan system for the three sets of clustered calcifications setting in breast tissue mimicking Zerdine™.

To further evaluate the system performance in resolving microcalcifications, CIRS assisted us to construct three sets of microcalcifications with a base of 0.22 dB/cm/MHz Zerdine™:(A) 0.71 to 0.85 mm, (B) 0.42 to 0.45mm, and (C) 0.3 to 0.35mm. Each set of the custered microcalcifications consists of five elements. The images are shown in Figure 9. In Figure 10, small calcifications in group (C) were further analyzed. We conclude that 3 out of 5 calcifications at 0.3mm range were resolvable.

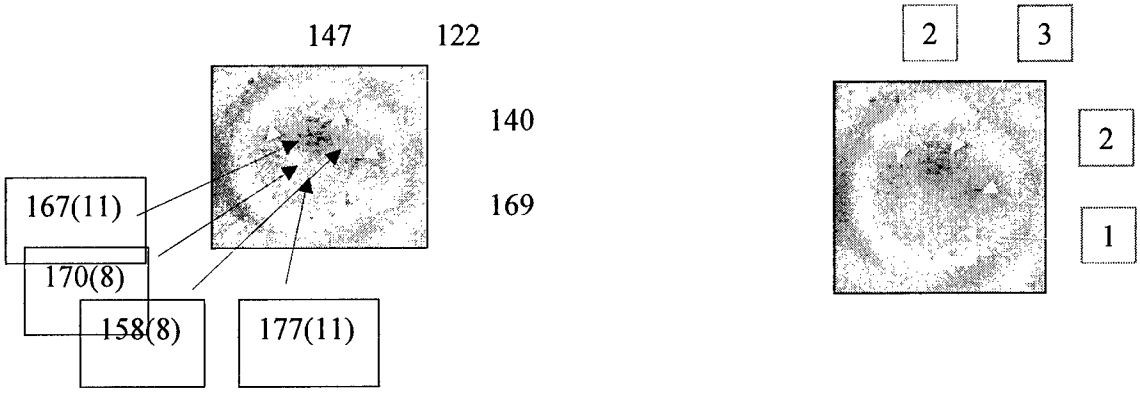

(A) Four intensity measures for the calcifications shown on the upper-right corners and the intensity (noise level) measures at selected background areas

(B) Estimated CNR values of the four calcifications. The numbers are the computed CNRs of the ROIs.

Figure 10. ROIs and their intensities and CNRs measures for the smallest clustered calcifications shown in Figure 9(C).

3.3. Real-time Image Sequencing using a Biopsy Simulation Phantom

We have also performed tests using breast phantoms containing simulated breast abnormalities including tumors and cysts. Again, each image was extracted from a single frame (1/30 second) of the sequential images without post-processing. Figure 11 shows a sequence of needle biopsy images using a CIRS phantom (Model 52) acquired from the C-Sacn prototype. The phantom has been used for training resident for sometime. A 2-cm tumor in the phantom was used as a model in the second part of the experiment. Figure 12 demonstrated several focal plane fields of the same detail obtained as one focuses from the edge into the center of the simulated. Each image contains a black boundary representing the region outside of the field of view of the transducer disk. Within this boundary is a lighter gray area which represents the background material of the phantom which surrounds the spherical details. The darker region in the center represents the spherical detail in the phantom. As we focus into the object, the cross section of the spherical object becomes larger as expected as one slices a sphere from its edge. The black linear streaks are the needle tracks. The white streaks are, we believe, based on a mammographic x-ray image, areas of leakage of the material from the spherical objects.

The use of ultrasound in image guided needle biopsy has been hindered by the physics of pulse echo ultrasound. In the use of conventional pulse echo ultrasound for breast biopsy, the needle must be kept in a perpendicular orientation to the ultrasound transducer. As the needle departs from this orientation it "disappears" because the pulse echo is scattered at angles other than the return angle which can be detected by the ultrasound transducer. The device discussed herein resolves this problem through the use of a transmission mode of ultrasound propagation. In transmission mode, ultrasound projects through the target volume in the same manner as x-ray. The detection of ultrasound through the target volume is not sensitive to orientation of the target as it is in pulse echo mode.

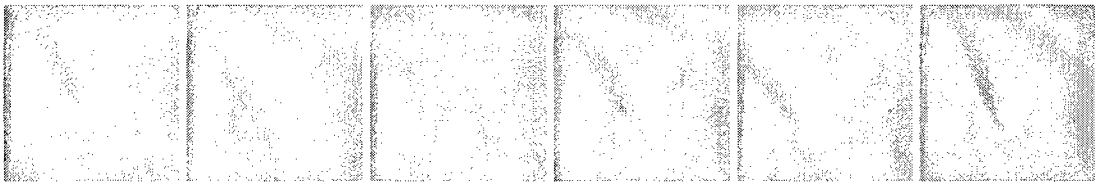

(A) (B) (C) (D) (E) (F)

Figure 11. The above images were sampled from a sequence of 150 ultrasound images taken from 30 frames per second for five seconds of a CIRS breast phantom. The camera focused on two small simulated masses and a biopsy needle about 4 cm below the surface. The needle first punctured the target (A) and (B), then left (C), and punctured the target again (D) and (E). The needle was rotated clockwise from (E) to (F). This operation pushed the mass on the right upper corner out of the focal plane.

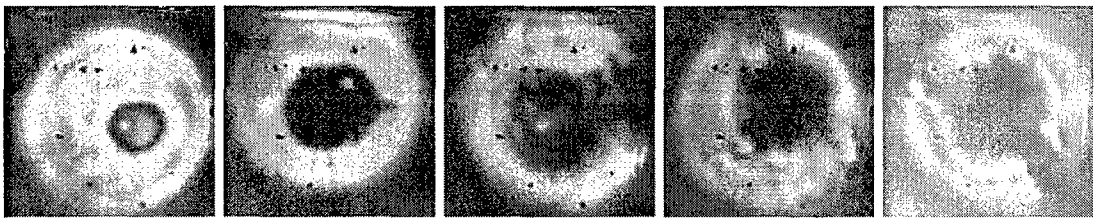

(A) (B) (C) (D) (E)

Figure 12. These images are of a specific detail in the Computerized Image Reference System (CIRS) breast ultrasound phantom Model 52 designed for tissue equivalent ultrasound needle biopsy training. The imaged detail is a spherical echogenic object simulating solid tumor within the phantom. The detail has been punctured multiple times under ultrasound guidance.

4. CONCLUSIONS AND DISCUSSION

In summary, we found the prototype system based on this hybrid microelectronic array that is capable of generating ultrasound images with fluoroscopy-like presentation, and significant contrast and spatial resolution. Our resolution study indicates that a spatial resolution at 250μm was observable using a fan-line phantom. Calcifications of equal to or greater than 350μm were observable. The contrast resolution study indicated the system is capable of differentiating objects 3mm in size with low differential contrast. The difference between the target and background materials in this experiment as low as 0.07 dB/cm/MHz.

The potential for use in biopsy procedures is demonstrated through the imaging of breast phantoms with simulated tumors. Two aspects of ultrasound guided biopsy procedures which hinder the performance of the procedure are speckle which hide abnormalities and the phenomenon of the "disappearing needle" as the orientation of the biopsy needle to the ultrasound transducer shift. Both of these problems are eliminated in the ultrasound imaging system discussed in this paper.

The new ultrasound images appear with no speckle artifact with fluoroscopy-like presentation. The images show no obvious geometrical distortion. Its high-resolution capability with outstanding features has attracted great research interests. Clinical investigation of the system is in-progress.

REFERENCES

1. L. Tabar and P. B. Dean: *Teaching Atlas of Mammography*. 2nd Ed., Thieme, NY, 1985.
2. E. A. Sickles, "Mammographic features of 300 consecutive nonpalpable breast cancers," AJR, vol. 146, p. 661, 1986.
3. F. M. Hall, J. M. Storella, D. Z. Silverstone, and G. Wyshak, "Nonpalpable breast lesions: recommendations for biopsy based on suspicion of carcinoma at mammography," Radiology, vol 167:353, 1988.
4. S. D. Frankel, E. A. Sickle, B. N. Curpen, R. A. Sollitto, S. H. Ominsky, and H. B. Galvin, "Initial versus subsequent screening mammogarphy: Comparison of findings and their prognostics significance," AJR, vol. 164, pp. 1107-1109, 1995.
5. C. J. Baines, A. B. Miller, C. Wall, et al. "Sensitivity and specificity of first screen mammography in the Canadian National Breast Screening Study: A preliminary report from five centers," Radiology, vol. 160:295, 1986.
6. R. E. Bird, T. W. Wallace, and B. C. Yankaskas, "Analysis of cancers missed at screening mammography," Radiology, vol. 184, No. 3, pp. 613-617, 1992.
7. L. Landini, R. Sarnelli, F. Squantini, "Frequency-dependent attenuation in breast tissue characterization," Ultrasound Med. Biol. Vol.11, pp. 599-603, 1985.
8. G. McDaniel, "Ultrasonic attenuation measurements on excised breast carcinoma at frequencies from 6 to10 MHz," Ultrasonic Symp. Proc. IEEE. Cat. No. 77CH1264-ISU, 234-236, 1977.
9. M. Ohori, T. M. Wheeler, P. T. Sardino, "The New American Joint Committee on Cancer and International Union Against Cancer TNM Calssification of Prostate Cancer, CANCER, Vol. 74(1), pp. 104-114, 1994.
10. T. A. Stamey, "Diagnosis of Prostate Cancer – A personal review" (Editorial), J. Urology, vol. 147, pp. 830-832, 1992.
11. K. Shinohara, T. M. Wheler, and P. T. Scardino, " The Appearance of Prostate Cancer on transrectal Ultrasonography: Correlation Imaging and Pathological Examinations," J. Urology, 142, p.76, 1989.
12. E. S. de Paredes, L. P. Marsteller, B. V. Eden, "Breast cancers in women 35 years of age and younger: Mammographic findings," Radiology, vol. 177, pp. 117-119, 1990.
13. L. W. Bassett and C. Kimme-Smithe, "Breast Sonography", AJR, Vol. 156, pp.449-455, 1991.
14. V. P. Jackson, R. E. Hendrick, S. A. Feig, and D. B. Kopan, "Imaging of Radiographically Dense Breast," Radiology, Vol. 188, pp. 297-301, 1993.
15. A. Ishisaka, H. Ohara, and C. Honda, " A New Method of Analysis Edge Effect in Phase Contrast imaging with Incoherent X-rays," Optical Review, Vol. 7, No. 6, pp.566-572, 2000.

*lo@isis.imac.georgetown.edu **lasserm@imperiuminc.com

Projection Ultrasound and Ultrasound CT using A PE-CMOS Sensor: A Preliminary Study

Chu Chuan Liu[1,2], Shih-Chung B. Lo[1], Matthew T. Freedman[1], David Rich[3], John Kula[3], Bob Lasser[3] and Marvin E. Lasser[3], JianChao Zeng[4], Doug Ro[5]

1. ISIS Center, Radiology Department, Georgetown University Medical Center, Washington, DC
2. Department of Electrical Engineering, Virginia Polytechnic Institute and State University, VA
3. Imperium Inc. Silver Spring, MD
4. Department of Electrical and Computer Engineering, Howard University, Washington, DC
5. Radiology Department, Virginia Commonwealth University Health System, Richmond, VA

ABSTRACT

The purpose of this study is to investigate the feasibility of generating 3D projection ultrasound computed tomography images using a transmission ultrasound system via a piezoelectric material coated CMOS ultrasound sensing array. There are four main components in the laboratory setup: (1) a transducer operated at 5MHz frequency generating unfocused ultrasound plane waves, (2) an acoustic compound lens that collects the energy and focuses ultrasound signals onto the detector array, and (3) a CMOS ultrasound sensing array (Model I100, Imperium Inc. Silver Spring, MD) that receives the ultrasound and converts the energy to analog voltage followed by a digital conversion, and (4) a stepping motor that controls the rotation of the target for each projection view. The CMOS array consists of 128×128 pixel elements with 85μm per pixel. The system can generate an ultrasound attenuation image similar to a digital image obtained from an x-ray projection system. A computed tomography (CT) study using the ultrasound projection was performed. The CMOS array acquired ultrasound attenuation images of the target. A total of 400 projections of the target image were generated to cover 180° rotation of the CT scan, each with 0.45° increment. Based on these 400 projection views, we rearranged each line profile in the corresponding projection views to form a sinogram. For each sinogram, we computed the cross section image of the target at the corresponding slice. Specifically, the projection ultrasound computed tomography (PUCT) images were reconstructed by applying the filtered back-projection method with scattering compensation technique. Based on the sequential 2D PUCT images of the target, we generated the 3D PUCT image.

Keywords: Ultrasound Computed Tomography, Ultrasound sensor array, and Transmission ultrasound.

1. INTRODUCTION

Recently Imperium Inc. has developed a piezoelectric material layer deposited onto a microarray chip through semiconductor processing based on Complementary Metal-Oxide Semiconductor (PE-CMOS) technology. The array is responsive over a wide range of ultrasound frequencies, although most imaging is done using frequencies ranging between 1MHz and 15MHz. We have setup a laboratory prototype to investigate the potential and found that this novel two-dimensional ultrasound attenuation imaging system can generate real-time, high-resolution, speckle-free images including subsurface structures in the breast[1]. Substantial improvements in physical performance of the imaging system based on the newly developed chip (model I400) have been made and will be reported[2].

Clinically, ultrasound has been used in assessing dense breast regions and in distinguishing between cysts and solid masses. It many situations, it has also been used as an image modality to guide needle biopsy of breast lesions. Due to the limitations of the ultrasound transmission and its refraction/absorption characteristics at the interface of the tissue, bone, and air, ultrasound computed tomography system developments have always been attempted to image the human breast for medical applications. Shortly after the first few generations of x-ray computed tomography were developed in the 1960s and 1970s, several investigators began to investigate the possibility of using ultrasound to generate ultrasound-based computed tomography. Greenleaf and his colleagues at Mayo Clinic were likely to be the first research team who successfully developed an ultrasound tomography system using transmitter-receiver pairs with a translation/rotation gantry similar to parallel-beam x-ray CT geometry to generate ultrasound CT images[3,4,5,6]. Later

Medical Imaging 2004: Ultrasonic Imaging and Signal Processing,
edited by William F. Walker, Stanislav Y. Emelianov, Proc. of SPIE Vol. 5373
(SPIE, Bellingham, WA, 2004) · 1605-7422/04/$15 · doi: 10.1117/12.537672

they also developed ultrasound diffraction tomography[7]. In the 1990s, André and his colleagues performed a significant amount of work on ultrasound diffraction tomography[8,9,10,11]. Recently, several investigators have reported various system developments in the field of ultrasound computed tomography including: Liu, Waag et al in Rochester[12], Marmarelis et al at University of Southern California[13], Lettrup, Leach et al in Detroit[14,15], and Johnson et al in Salt Lake City[16]. In addition, a substantial 3D ultrasound computed tomography system was developed in Germany and led by Stotzka[17]. In this study, we performed a preliminary study to show that a 3-D projection ultrasound computed tomography could be generated using the CMOS ultrasound sensor. Since our system apparatus is quite simple and inexpensive and the image resolution is much higher, this ultrasound computed tomography system has substantial clinical implications.

2. MATERIAL AND METHODS

2.1. The System Configuration of the Transmission Ultrasound

To generate real-time images, ultrasound is introduced into the object under study with a large unfocused plane wave source. The ultrasound wave transmits through the object and is attenuated and scattered. The acoustic lens collects the transmitted energy and focuses it onto the sensing array.

The sensing array is made up of two components, a silicon detector/readout array and a piezoelectric material that is deposited onto the CMOS array through semiconductor processing. The active size of PE-COMS array is 1 cm square consisting of 128×128 pixel elements (16,384) with 85μm pixel spacing. Hence, a circular area covering up to 3 inches in diameter can be imaged onto the sensor. The array is responsive over a wide range of ultrasound frequencies, although most imaging is done using frequencies ranging between 1MHz and 10MHz.

The system operates by pulsing a commercial off-the-shelf ultrasonic spike pulser. A plane wave enters the target, scatters, exits the target and gets into the acoustic lens, which collects the scattered energy and focuses it onto the array. This operation repeats 30 times/second. Standard video electronics and image processing are used to format the image for presentation to the user and can perform real-time image display either on a PC monitor or on a hand held LCD. Figure 1 shows the system configuration of the projection ultrasound. Figure 2 shows our laboratory setting. The sensing microarray and the ultrasound source are located in the left and right sides of the water tank, respectively.

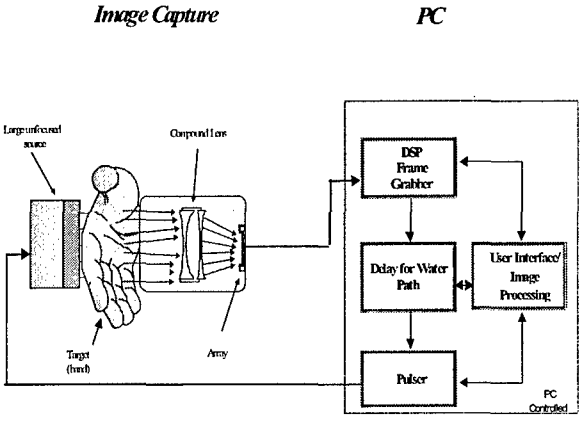

Figure 1. The system configuration

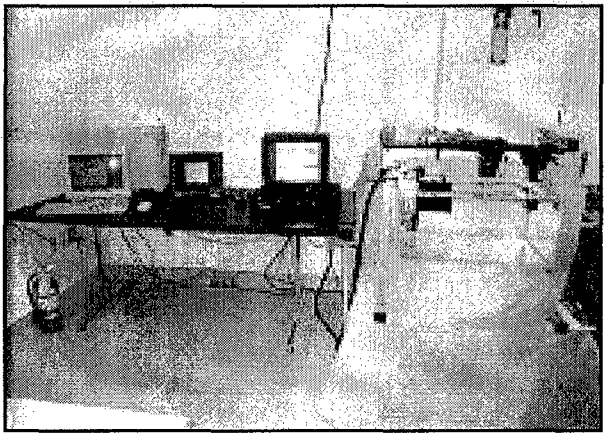

Figure 2. The PUCT system

2.2. General Performance of the Ultrasound Imaging System[1]

The images generated by the system appear to have no speckle with fluoroscopy-like presentation. The images show no obvious geometrical distortion. Our experimental results indicated that the system has a spatial resolution of ~0.32 mm using a fan-wire phantom. It can detect simulated breast lesions smaller than 3mm with low contrast (i.e., attenuation coefficient difference is less than 0.07dB/cm/MHz) in). It can detect microcalcifications smaller than 0.42mm. All these results were obtained when the objects were imbedded in a 6cm thickness of breast tissue mimicking phantoms (CIRS custom made phantoms with Zerdine™ background at 0.22dB/cm/MHz). We have also taken some

attenuation ultrasound images using the projection ultrasound system for various medical applications. Two sample images are shown below: a breast tissues image in Figure 3 and a prostate tissue attenuation image in Figure 4.

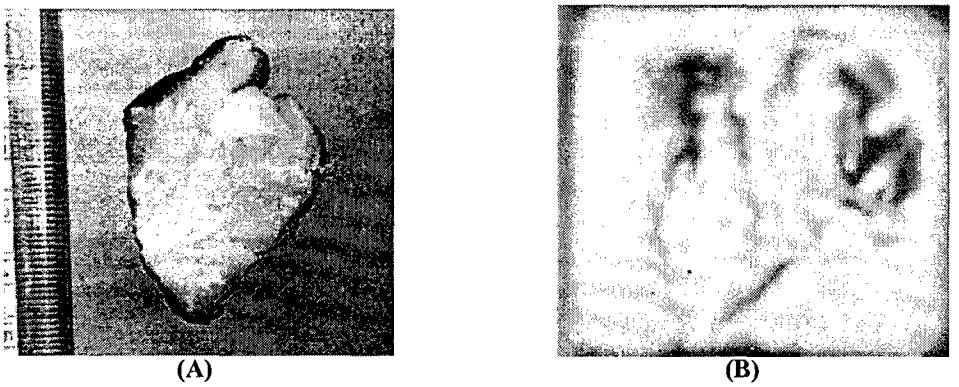

(A) (B)

Figure 3. (A) A breast tissue specimen and (B) An ultrasound attenuation image of the breast specimen.

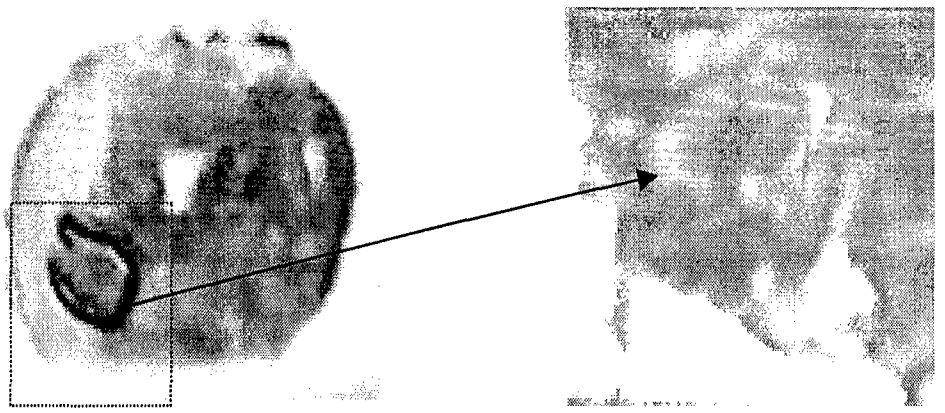

(A) (B)

Figure 4. (A) A prostate tissue specimen and (B) An ultrasound attenuation image of the prostate specimen.

2.3 Compensation of Inactive Pixels

The sensing array possesses a few inactive pixels as other CMOS-based sensing array that produces white or black dots on the image. As a part of image pre-processing, we first took a background image (without using ultrasound). Then we applied a point detector filter to mark the locations of inactive pixels. After we located those inactive pixels, a bilinear interpolation method was applied for the compensation of those pixels. A set of sample image with human finger is shown in Figure 5.

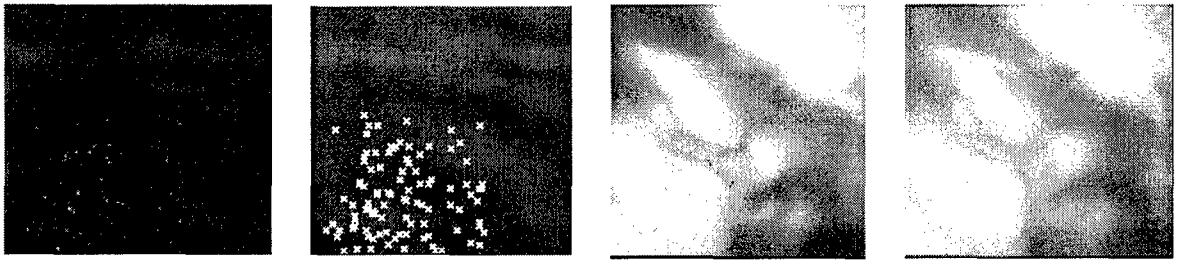

(A) (B) (C) (D)

Figure 5. (A) Inactive pixels. (B) Marked inactive pixels. (C) Original images. (D) Processed images.

3. PUCT EXPERIMENT AND RESULTS

3.1 PUCT System Setup

The detailed look of our PUCT system is shown in Figure 6. The top of the water tank contains the micro-stepping motor controller and its power supply. The maximum resolution of the micro-stepping motor is 800 steps in 180° rotation. In our experiment, we generated 400 projections for a 180° rotation. On the left of the water tank, the sensing array is contained in a metal box and mounted with a compound acoustic lens. In the center, the target is directly connected to the stepping motor for rotation. The 5MHz ultrasound plane wave transducer is located on the low-right side of the picture.

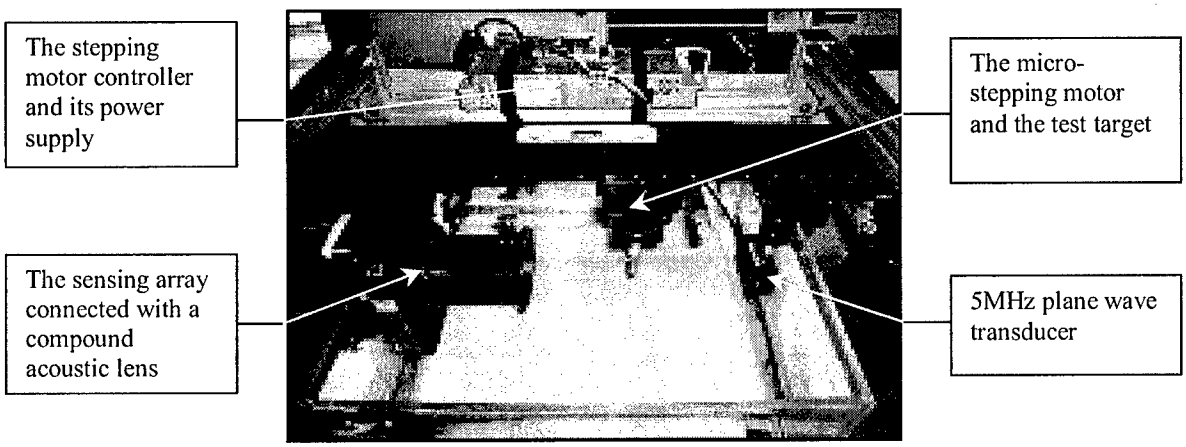

Figure 6. Close view of the PUCT system setup

3.2 Test Targets

For the purpose of studying the possibility in generating ultrasound computed tomography images, we made two targets for PUCT experiment using silicone, plastic based pearl shape objects, plastic tubes and metal wires as shown in Figure 7 (A). The test targets are about ½ inch in diameter and 3 inches in length with a cylinder shape. We inserted 3mm pearl object in one phantom (see Figure 7(B)) and 2mm objects and a wire with 0.6mm in diameter in another phantom (see Figure 7(C)). The center section slice of test target No.1 and No.2 with their projection images are shown in Figure 7.

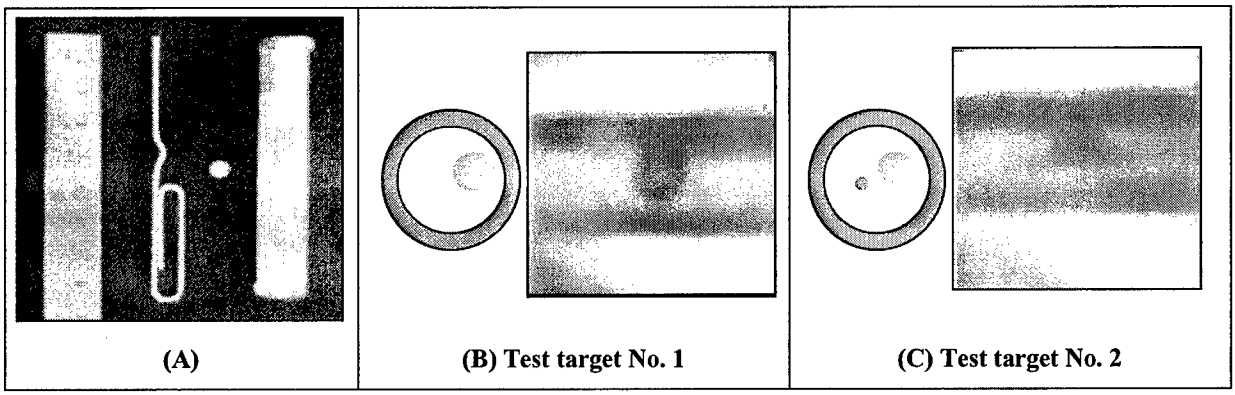

Figure 7. (A) The test target and its contents. (B) The center cross section slice of test target No.1 in drawing and its projection ultrasound attenuation image at view angle 0°. (C) The center cross section of test target No.2 in drawing and its projection ultrasound attenuation image at view angle 0°.

3.3. Ultrasound Attenuation in Projection Geometry

The fundamental assumption of ultrasound as it transmits through materials is that the ultrasound intensity is attenuated based on exponential decay along the propagation path. In this experiment, we first acquired an image without any target as the initial intensity, $I_0(z,t)$. With the test target, we acquired 400 projection images, $I(z,t,\theta)$, to cover 180° rotation. This was done by imaging the target with an angle increment of 0.45° for each rotation step. Then we applied the projection attenuation function to obtain the attenuation images:

$$p(z,t,\theta) = -\log\left(\frac{I(z,t,\theta)}{I_o(z,t)}\right) \qquad \ldots(1)$$

where $p(z,t,\theta)$ is the attenuation for pixel location (t,θ) for rotation view θ.

With our tube phantom, made by the plastic wall and silicone, a "W" shape attenuation profile in one-dimension is expected without considering other physical processes. As shown in Figure 8, ultrasound waves pass through more plastic material on the edge of the tube and receive higher attenuation than the center section of the test target.

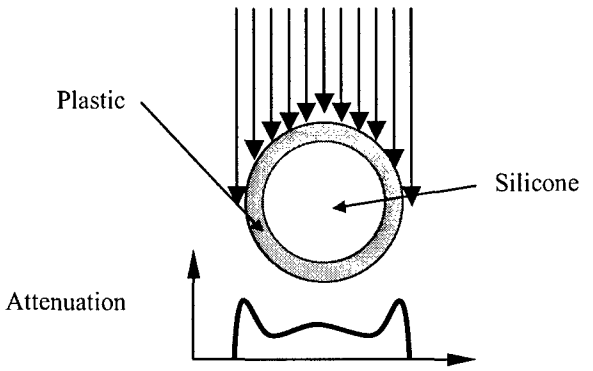

Figure 8. The attenuation distribution of the test target with primary ultrasound wavefront.

3.4. Initial PUCT results

Based on the attenuation profiles, we arranged each vertical line of the sensing array to form the sinogram (Figure 9) for each cross section slice and prepared for filtered backprojection process. A sinogram contains the line attenuation profile from the 400 projections. Since low noise is expected for a small test object, we applied a standard theoretical filter (i.e., Ram-Lak filter) for the filtered backprojection reconstruction[18]:

$$f(z,x,y) = \frac{1}{4\pi^2}\int_{-\infty}^{\infty}\int_{-\infty}^{\infty} P(z,\phi,\omega)e^{j2\pi(x\sin\phi + y\cos\phi)}\,|\omega|\,d\omega\,d\phi \qquad \ldots(2)$$

where $P(z,\phi,\omega) = FT\{p(z,\theta,t)\}$ and $p(z,\theta,t)$ is the profile. The initial results for test targets No.1 and No.2 are shown in Figure 10 (A) and (B) respectively. Each PUCT image represents a slice of the target in the position of the dash line on the projection image. The outer bright ring (the plastic tube) is clearly shown. However, the pearl shaped object is barely observable. The center part of the PUCT image suffers a circular shadow effect from the ultrasound scattering. This effect is commonly encountered when a planar detector is employed[19].

3.5. Circular Shadow and the Correction Method

In order to correct the shadowing effect, we modeled the shadow image so that only the shadow frame was used. This process attempted to compensate for the base attenuation distortion. Figure 11 (A) and (B) are the attenuation shadow frame and its inversed image, respectively. We then applied computer re-projection[20] as shown in Figure 11 (C) to generate attenuation correction profiles for all 400 views.

(A) (B)

Figure 9. Sinograms of test target No.1 (A) and test target No.2 (B).

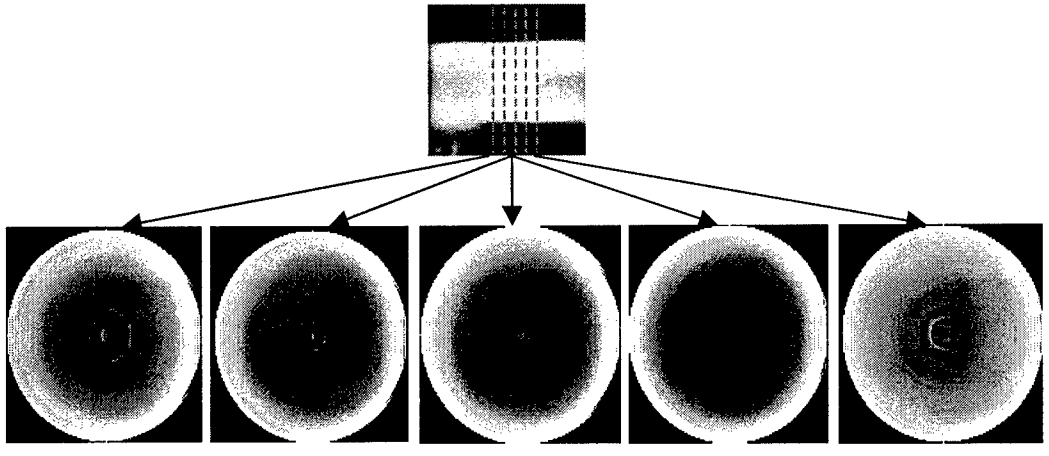

(A)

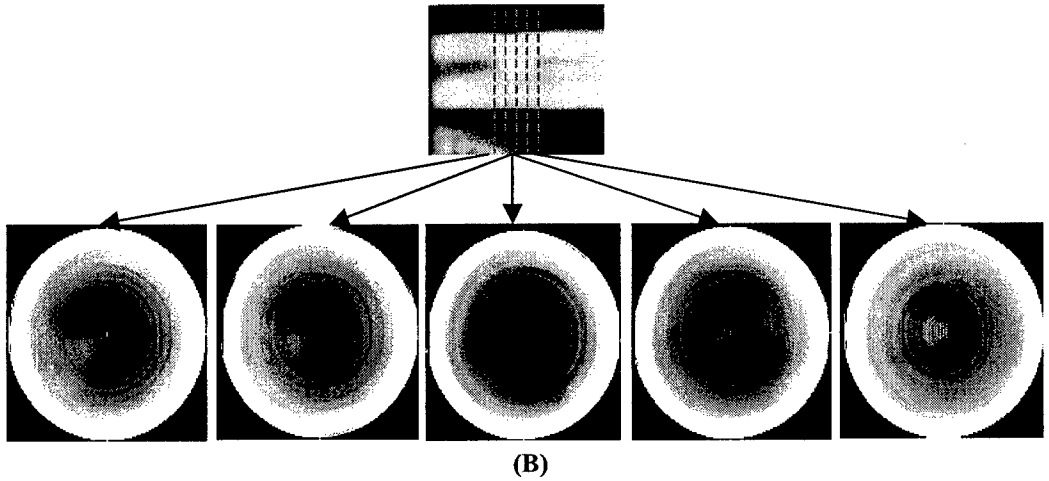

(B)

Figure 10. (A) Initial UCT results for test target No.1. (B) Initial UCT results for test target No. 2.

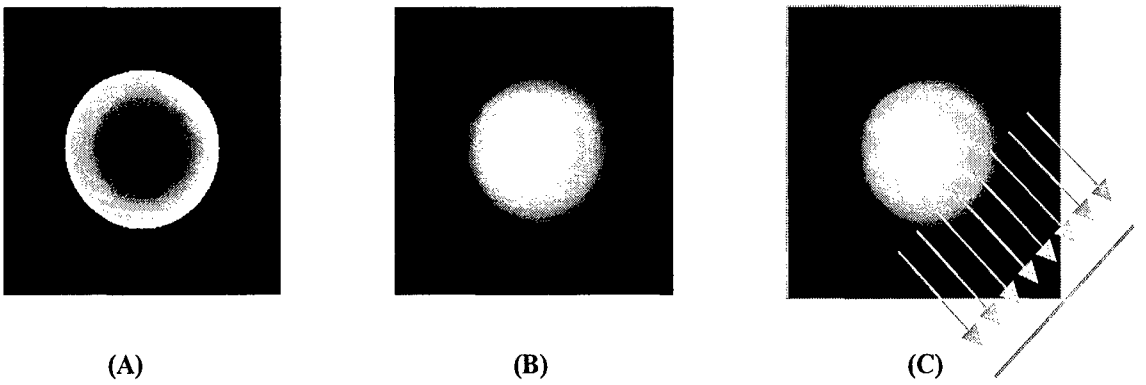

(A) (B) (C)

Figure 11. (A) The circular shadow model, (B) its inversed image, and (C) computer reprojection method.

The inversed shadow profiles are obtained as

$$p_s(z,t,\theta) = \int_{(t,\theta)} IS(x,y)da \qquad ...(3)$$

where IS(x,y) is the inversed shadow, "a" is the integration path that is perpendicular to the profile direction "t". Then the filtered backprojection reconstruction was applied on the compensated attenuation profile as

$$f_c(z,x,y) = \frac{1}{4\pi^2} \int_{-\infty}^{\infty} \int_{-\infty}^{\infty} (P_c(z,\phi,\omega) e^{j2\pi(x\sin\phi + y\cos\phi)} \mid \omega \mid d\omega d\phi \qquad ...(4)$$

where $P_c(z,\phi,\omega) = DFT\{p_c(z,\theta,t)\}$ and $p_c(z,\phi,\omega) = p(z,\theta,t) + p_s(z,\theta,t)$.

3.6. Scattering Corrected PUCT Results

After the computer produced re-projection for the intensity profile, we corrected the original sinogram using the re-projection sinogram. Then the filtered backprojection process for each corrected sinogram was performed again. The scattering corrected PUCT reconstructed images are shown in Figure 12. By comparing the corresponding images in Figure 12, the circular shadow effect is significantly reduced among all scattering corrected PUCT images. In addition, the structures of the test objects inside the target (i.e., pearl shape object and the wire) are significantly improved. As shown in Figure 12 (B), it is seen that the wire on the left slices of the projection appear closer to the center while cutting the slices toward the right side of the projection. In addition, it is seen that the pearl shape object is correctly located in the right side of the cross section PUCT image corresponding to the center projection image. However, some ring artifacts appear on the center of the PUCT images which were due to the inconsistency of the center of rotation during the PUCT scan experiment. The ring artifacts could have been avoided if less than a submillimeter shift of the object was maintained. However, a more sophisticated rotating apparatus was needed to achieve this system requirement.

4. CONCLUSIONS AND DISCUSSION

In this paper, we demonstrated that the PE-COMS sensing array is capable of generating real-time speckle-free attenuation ultrasound images and is also capable of producing 3D projection ultrasound computed tomography images. Basic system performance of the sensor array when the used in projection geometry has been presented in our previous paper[1]. Updated system performance with newly fabricated chip (Model I400, Imperium Inc, Silver Spring, MD) will be reported soon.

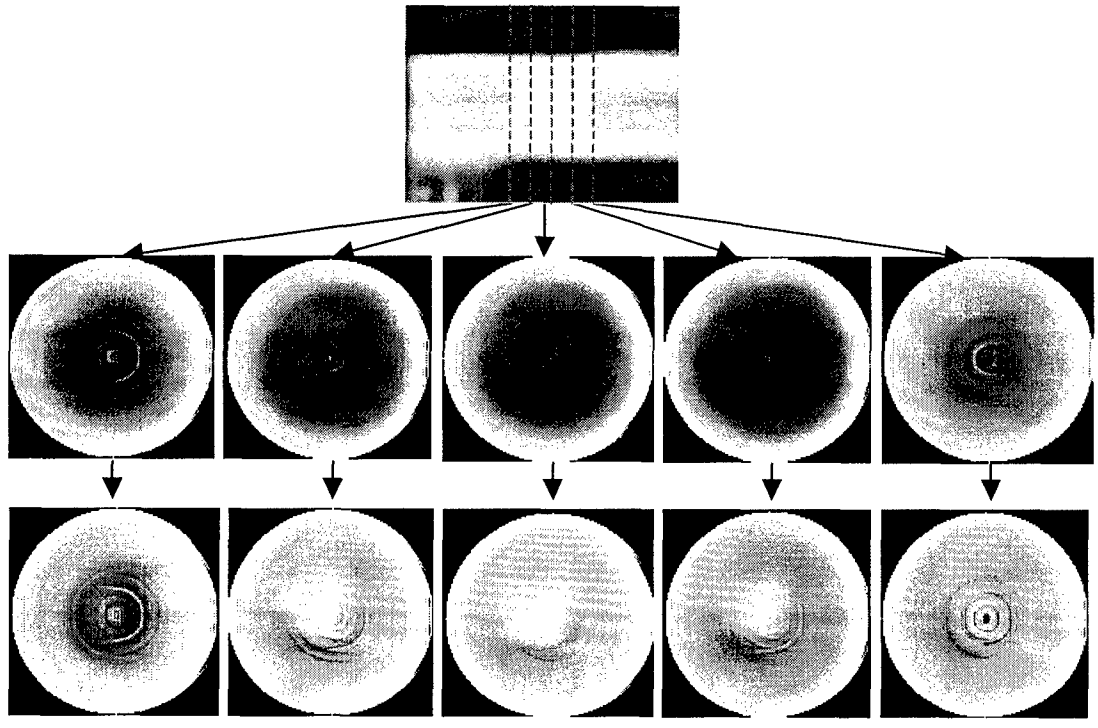

(A) The PUCT reconstruction image sequence of test target No.1.

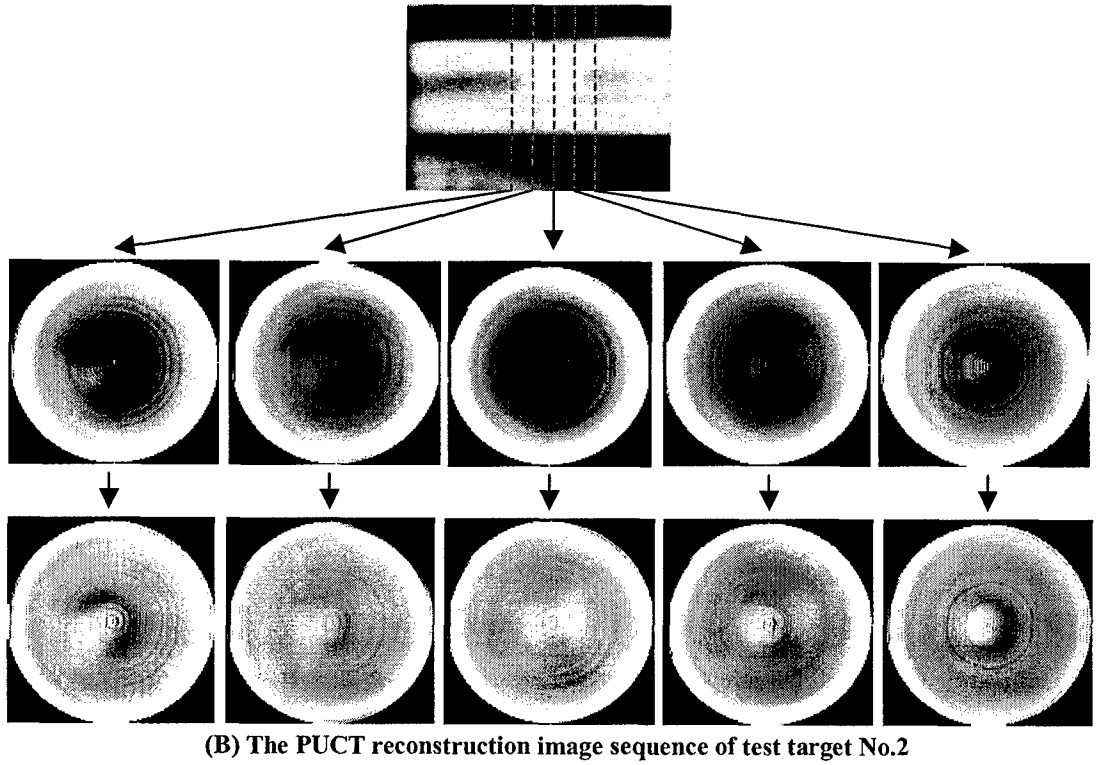

(B) The PUCT reconstruction image sequence of test target No.2

Figure 12. Comparison of the initial result and the scattering corrected images for the two test targets.

During the PUCT experiment, we encountered several potential artifacts as those experienced in x-ray CT system developments including cone beam CT systems[18]. Obvious artifacts include (1) circular shadow due to scattering on the planar array, (2) ring artifact due to off-center rotating during the PUCT rotation/projection scan, and (3) beam hardening effect due to the high attenuation of the object. For the issue of the circular shadow effect, we successfully applied the computer re-projection technique on the scattering model to significantly overcome the shadow. The scattering corrected PUCT images reveal the structures of small objects in the test target. However, we found that a more accurate rotating frame is needed in order to avoid ring artifacts.

ACKNOWLEDGMENTS

This work was supported in part by an US Army research grant (No. DAMD17-0101-0197) and an NIH/NIBIB Grants (No. EB002130).

REFERENCES

1. S-C.B. Lo, D. Rich, M.E. Lasser, J. Kula, H. Zhao, R. Lasser, and M.T. Freedman, "A C-Scan Transmission Ultrasound Based on a Hybrid Microelectronic Sensor Array and Its Physical Performance," SPIE Proc. Med. Img. Vol. 4325, pp. 89-95, 2001.
2. S-C.B Lo, C. Liu, D. Rich, J. Kula, R. Lasser, M.E. Lasser, M.T. Freedman, and J. Gurney, "A Highly Sensitive PE-COMS ultrasound sensor and Its Clinical Implications," Med. Physics. (Submitted for review 2004).
3. J.F. Greenleaf, S.A. Johnson, and A.H. Lent, "Measurement of spatial distribution of refractive index in tissues by ultrasonic computer-assisted tomography." Ultrasound in Medicine and Biology, (3): 327-339, 1978.
4. J.F. Greenleaf, S.K. Kenue, B. Rajagopalan, R.C. Bahn, and S.A. Johnson, "Breast imaging by ultrasonic computer-assisted tomography," Acoustical Imaging, volume 12, pp. 599-614, 1980.
5. J.F. Geenleaf, J. Ylitalo, and J.J. Gisvold, "Ultrasonic computed tomography for breast examination." *IEEE* Engineering in Medicine and Biology Magazine, 6(4): 27-32, December 1987.
6. J.S. Schreiman, J.J. Gisvold, J.F. Greenleaf, and R.C. Bahn, "Ultrasound transmission computed tomography of the breast." *Radiology*, 150(2):523-530, February 1984.
7. B.S. Robinson and J.F. Greenleaf, "An experimental study of diffraction tomography under the Born approximation," Acoustical Imaging, *volume 18*, pp. 391-400, 1991.
8. M.P. André, H.S. Janee, T.K. Barrett, B.A. Spivey, P.J. Martin. "Simultaneous spatial and velocity vector mapping with diffraction tomography." Acoustic Imaging, 1997, Vol. 23, pp. 583-588.
9. C.D. Lehman, M.P. André, B.A. Fecht, J.M. Johansen, R.L. Shelby. "Through transmission US applied to breast imaging". Academic Radiology. 7(2): 100-107, 2000.
10. M.P. André, H.S. Janee, G.P. Otto, P.J. Martin, "High speed data acquisition in a diffraction tomography system with large-scale toroidal arrays" Int J Imaging Systems Tech., 1997, Vol. 8. No. 1, pp. 137-147.
11. M.P. André, H.S. Janée, G.P. Otto, P.J. Martin, M.Z. Ysrael. "Diffraction tomography breast imaging system: Patient image reconstruction and analysis". Acoustical Imaging. 24: 325-334, 2000.
12. D. L. Liu and P. C. Waag "Propagation and backscattering for Ultrasonic wavefront design," IEEE Tran. On Ultras. Ferro., and Freq. Contr. 44(1):1-13, 1997.
13. V.Z. Marmaralis, T. Kim, R.E. Shehada, "High Resolution Ultrasound Transmission Tomography", Proceeding of the SPIE Medical Imaging 2003, Vol. 5035.
14. P.J. Littrup, N. Duric, S. Azevedo, D.H. Chamber, J.V. Candy, S. Johnson, G. Auner, J. Rather, and E.T. Holsapple, "Computerized Ultrasound Risk Evaluation (CURE) System: Development of Combined Transmission and Reflection with New Reconstruction Algorithm for Breast Imaging," Proc. Of International Acoustical Imaging Symposium, Windsor, Canada, Sept. 2001.
15. R.R. Leach Jr., S.G. Azevedo, J.G. Berryman, H.R. Bertete-Aguirre, D.H. Chambers, J.E. Mast, P.J. Littrup, N. Duric, F. A Wuebbeling "Comparison of ultrasound tomography methods in circular geometry". Proceedings of he SPIE: Medical Imaging 2002; San Diego, California; Feb. 23-28, 2002. Ultrasonic Imaging and Signal Processing - Paper 4687-44.
16. S.A. Johnson, D.T. Borup, J.W. Wiskin, F. Natter, F. Wuebbling, Y. Zhang, C. Olsen, "Apparatus and Method for Imaging with Wavefields using Inverse Scattering Technique". US Patent 6,005,916 (1999).
17. R. Stotzka, G. Gobel and K. Schlote-Holubek, "Development of transducer arrays for ultrasound-computertomography", "Ultrasound imaging and signal processing", Proceeding of the SPIE, Medical Imaging 2003, Vol 5035, pp. 513-520.
18. A. C. Kak and M. Slaney, " Principles of Computerized Tomographic Imaging ", IEEE Press, 1988, pp.49-75.
19. J. Wiegert, G. Rose, D. Schafer, M. Bertram, N. conrads, T. Aach, N. Noordhoek, "Soft tissue contrast resolution within the head of human cadaver by means of flat panel-based cone-beam CT", SPIE 2004, paper 5368-41.
20. S-C. B. Lo, "Strip and Line Path Integrals with Square Pixel Matrix - A Unified Theory for Computational CT Projections," IEEE Trans. Medical Imaging, Vol 7, No. 4, Dec. 1988, pp. 355-363.

Transmission and Reflective Ultrasound Images using PE-CMOS Sensor Array

Shih-Chung B. Lo[a], Chu Chuan Liu[a,b], Matthew T. Freedman[a],
John Kula[c], Bob Lasser[c], Marvin E. Lasser[c], Yue Wang[b]

a. ISIS Center, Radiology Department, Georgetown University Medical Center, Washington, DC
b. Department of Electrical Engineering, Virginia Polytechnic Institute and State University, VA
c. Imperium Inc. Silver Spring, MD

ABSTRACT

The purpose of this study is to investigate the imaging capability of a CMOS (PE-CMOS) ultrasound sensing array coated with piezoelectric material. There are three main components in the laboratory setup: (1) a transducer operated at 3.5MHz-7MHz frequency generating unfocused ultrasound plane waves, (2) an acoustic compound lens that collects the energy and focuses ultrasound signals onto the detector array, and (3) a PE-CMOS ultrasound sensing array (Model I400, Imperium Inc. Silver Spring, MD) that receives the ultrasound and converts the energy to analog voltage followed by a digital conversion. The PE-CMOS array consists of 128×128 pixel elements with 85μm per pixel. The major improvement of the new ultrasound sensor array has been in its dynamic range. We found that the current PE-CMOS ultrasound sensor (Model I400) possesses a dynamic range up to 70dB. The system can generate ultrasound attenuation images of soft tissues which are similar to digital images obtained from an x-ray projection system. In the paper, we also show that the prototype system can image bone fractures using reflective geometry.

Keywords: Ultrasound sensor array, Transmission ultrasound imaging, Reflective ultrasound imaging.

1. INTRODUCTION

Clinical interpretation of conventional ultrasound images requires special training in pattern recognition, a consequence of both the general acoustic heterogeneity of human organs and the similarity in acoustic properties between normal and abnormal tissues. Screening with ultrasound is difficult because operators depend upon thin tissue sections for image acquisition and visualization. The adequacy of image acquisition is significantly dependent upon the operator and difficulty in interpretation limits applications of ultrasound for non-expert medical team members. Furthermore, cross-sectional ultrasound is not efficacious in imaging extremities[1,2,3].

B-mode ultrasound has also been used to assess dense breast regions and to distinguish cysts from solid masses. It many situations, it has also been used as an image modality to guide needle biopsies of breast lesions. , Attempts to develop bone and air attenuation-based and distortion-free ultrasound due to the limitations of the ultrasound transmission and its refraction/absorption characteristics at the interface of the tissue

During the past several years, Imperium Inc has worked intensively to develop a higher sensitivity chip (Note: Model I400 is the newest version). We have intended to use the sensor as the basis for the development of an attenuation-based ultrasound system. This new ultrasound imaging device is fundamentally different from conventional B-mode ultrasound imaging regarding geometrical configuration, some physical characteristics of ultrasound, and signal acquisition. Conventional ultrasound imaging creates images based on the speed of the ultrasound signals traveling through tissues and then reflecting back to the receiver. The new ultrasound imaging device generates images based on tissue attenuation of the ultrasound signals in transmission mode. When it functions in a reflective mode, the image represents the composed effects of attenuation and reflection along the travel path. The new system, with its speckle-free and high-resolution capability, would add new parameters for analyzing tissue features in ultrasound imaging.

Medical Imaging 2005: Ultrasonic Imaging and Signal Processing,
edited by William F. Walker, Stanislav Y. Emelianov, Proc. of SPIE Vol. 5750
(SPIE, Bellingham, WA, 2005) · 1605-7422/05/$15 · doi: 10.1117/12.595615

2. MATERIAL AND METHODS

2.1. The Ultrasound Sensing System and Basic Image Acquistion Process

The sensing array is made up of two components: (1)a silicon detector/readout array and (2)a piezoelectric material that is deposited onto the CMOS array through semiconductor processing, hence it was named PE-CMOS sensor array. The active size of PE-CMOS array is 1 cm^2 with 128×128 pixel elements (16,384) and 85μm pixel spacing. The array is responsive over a wide range of ultrasound frequencies, although most imaging is done using frequencies ranging between 1MHz and 10MHz. Another key feature of this chip is the Readout Integrated Circuit (ROIC) that is attached to the center of the Pin Grid Array (PGA) as shown in Figure 1. This is a patented, custom-designed circuit that contains 120×120 cells or pixels. Each pixel contains the necessary circuitry to detect and capture the electrical signals that fall upon that pixel. Additional circuitry within the ROIC allows for the overall control and readout of the contents of the buffers that contain the data.

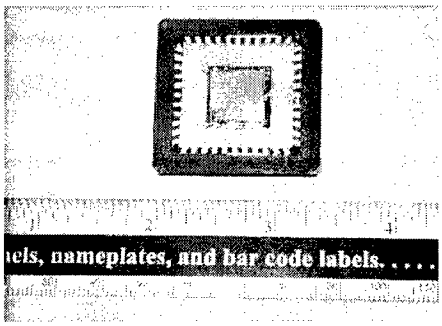

Figure 1. Photograph of the chip

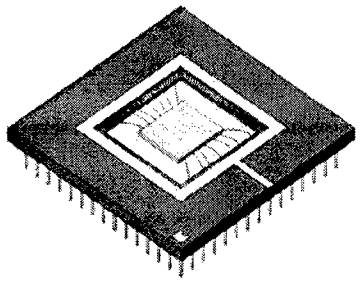

Figure 2. Schematic of the chip

When ultrasound impinges upon the I400 chip, the piezo-electric coating that makes up the chip's outer layer converts pressure to a time-varying signal that is amplified by a factor of 20 in the pre-amplifier. Next, a unique peak-detecting circuit is employed to detect the maximum signal within a selectable time window. This peak signal is then stored within a capacitor that is then emptied using a cup and bucket scheme that acts to increase the intra-frame SNR of the overall circuit. After this, the signal is corrected to account for non-uniformities, pixel-to-pixel, to result in a consistent field across the detector aperture. The corrected output is then stored within a buffer until it is emptied using a multiplexer circuit. This process results in the formation of image data, where each datum is rescaled to a 14-bit value.

The system operates by pulsing an ultrasonic spike pulser. This excites the large area ultrasound transducer (only used as a source) and sends a highly uniform plane wave through the water and/or media. This plane wave enters the target, scatters, exits the target and strikes the acoustic lens which collects the transmitted energy and focuses it onto the array. This operation repeats 30 times/second. Standard video electronics are used to format the images and to perform real time image acquisition and display.

The image acquisition process can be used in either the thru-transmission (TT) or pulse echo (PE) mode. We have designed a camera that can be placed in intimate contact with the test object using a special acoustic coupling gel or compliant pads or membranes. The TT mode is straightforward and may be thought of as illuminating the test object with a "flashlight" of US. It generally provides the most information and allows greater "penetration" of the test object with US. However, it requires access to both sides of the test object. For the one-sided case, it is necessary to use some form of the PE mode. In this mode of operation, the transducer US energy is scattered off the test object. Imperium Inc. has designed and built ultrasound image prototypes of both modes.

2.2. General Performance of the Ultrasound Imaging System

(A) Spatial Resolution

We have investigated the ability of the C-scan system to resolve separate objects. A custom-

fabricated phantom used in this investigation contains seven, 250 μm steel wires embedded in a fan shape. Figure 6 shows a PE-CMOS ultrasound image of this phantom. The intensity of the steel wires along the drawing line (not in the original image) is shown in Figure 7 as the lower intensity values and the gaps between the wires are shown as the higher intensity values. The average gap between the wires is ~350 μm. The images shown on Figures 3 & 4 may appear to be enhanced by the phase contrast because the phenomenon of phase contrast acts to enhance the edges of objects for projection imaging, where there is a large gap between object and detector[4,5]. Phase contrast can significantly improve resolution which is achievable beyond the limit.

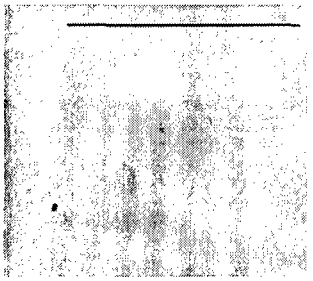

Figure 3. Image of a wire fan phantom

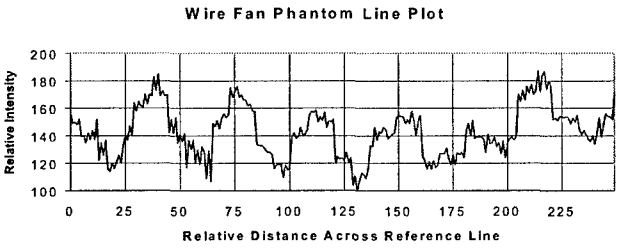

Figure 4. Line intensity plot (horizontal line shown in Fig. 3)

(B) MTF Measurement

A sample vertical edge image of 6cm Zerdium™ (0.21 dB/cm/MHz) was taken (see Figure 5). The image was acquired using a 5MHz broad band transducer. The gray region shows the same background of the wire fan phantom and the contrast phantom described above. The dark region represents the image that was blocked by a flat steel plate with a sharp edge. We took a sample data profile along the horizontal direction as an edge spread function and applies the derivative onto this data profile to obtain a line spread function. A noise reduction treatment was applied to the line spread function for the two sides of the edges. We then applied the Fourier Transform to the noise reduced line spread function and obtained the MTF. Both the line spread function and MTF of the system are shown in Figures 6 and 7, respectively. The results indicate that 70% of the full spatial frequency (62 lp/130 mm) can be reached for an MTF of 0.1, and 37% of the full spatial frequency can be reached for an MTF of 0.2. We therefore conclude that the system can resolve approximately 300 microns for an MTF of 0.1 when noise is suppressed. This result is quite close to that obtained using the fan-wire phantom.

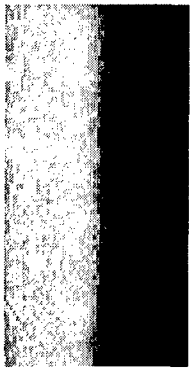

Figure 5. A vertical edge image

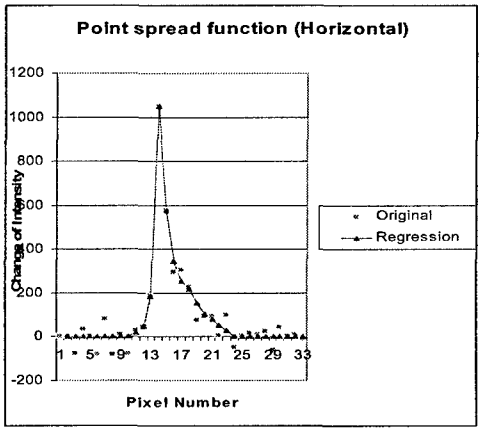

Figure 6. Plot of the line spread function and its regression.

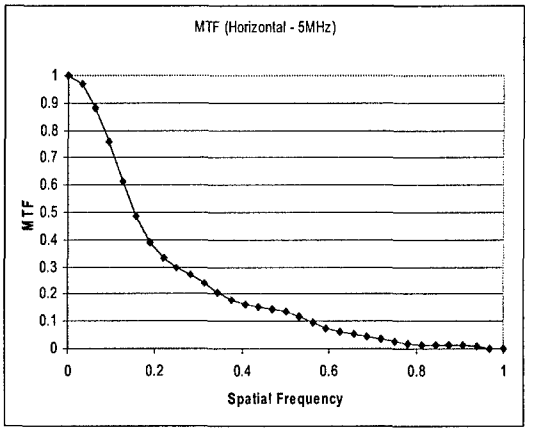

Figure 7. MTF of the imaging system (5MHz broad band transducer).

(C). Dynamic Range of the Ultrasound System

A CIRS custom made phantom containing clear background material and the white material as the step wedge was used to perform the dynamic range study. The phantom was moved to place the step to be imaged in the object plane. Fourteen images were acquired, including 13 from the dynamic range phantom and without the phantom. Mean and standard deviation values were measured for each attenuation step. The mean values were used to show the intensity response versus attenuation. In order to further investigate the attenuation effect of the measured intensity we examined the intensity response (I) by taking LOG as a function of the calculated attenuation.

$$AT = \text{Log}\left((I_o - I_b)/(I - I_b)\right) \qquad \ldots\ldots\ldots (1)$$

where I is measured intensity, I_o is the full intensity emitted from the transducer, and I_b is the intensity measure without any ultrasound signal (i.e. dark current in the chip). We found that the digital value of I_b is approximately 2600. We extrapolated the intensity function and found that the digital value of I_o is approximately 10,000. The LOG values of intensity ratio versus the calculated attenuation values in dB. The total attenuation for each step wedge and its corresponding intensity responses were computed and are shown in Figure 8. The LOG values of the intensity ratio are fairly linear with respect to the calculated attenuation more than 60dB when the system is operated at 5MHz. A linear response up to 70dB was found when the system operated at 7.5 MHz. The standard deviation values provide an indication of the uniformity of the pixel intensity. We found that the standard deviations of the digital values are generally lower than 3-4% of the mean intensity value.

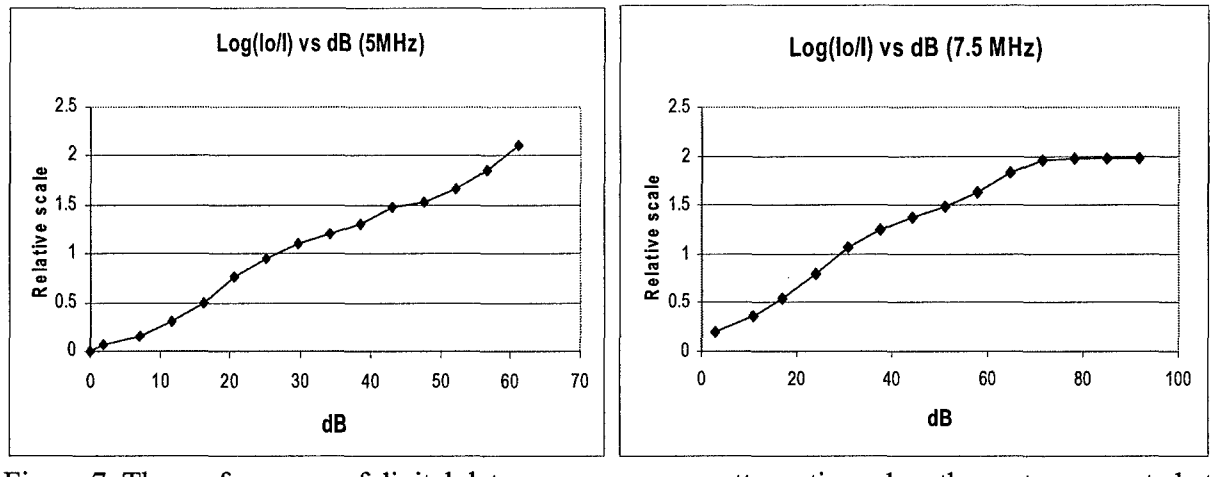

Figure 7. The performance of digital data response versus attenuation when the system operated at 5 MHz and 7.5MHz.

2.3. In vivo Images and Tissue Mimicking Images

It is convenient for us to investigate the finger images using the newly developed chip sensor (Imperium PE-CMOS model I400). Several images were taken using the 5MHz transducer and are presented in Figure 8. These images show clear structures of a finger. Due to the superior quality of these images in comparison to the images taken using the model I100, we began to identify the image patterns in the finger images. Figure 8(A)-(D) shows 4 regions of the finger and hand. When the 7.5MHz ultrasound transducer is used, many finer structures of the finger are clearly seen on the images as shown in Figure 8(E).

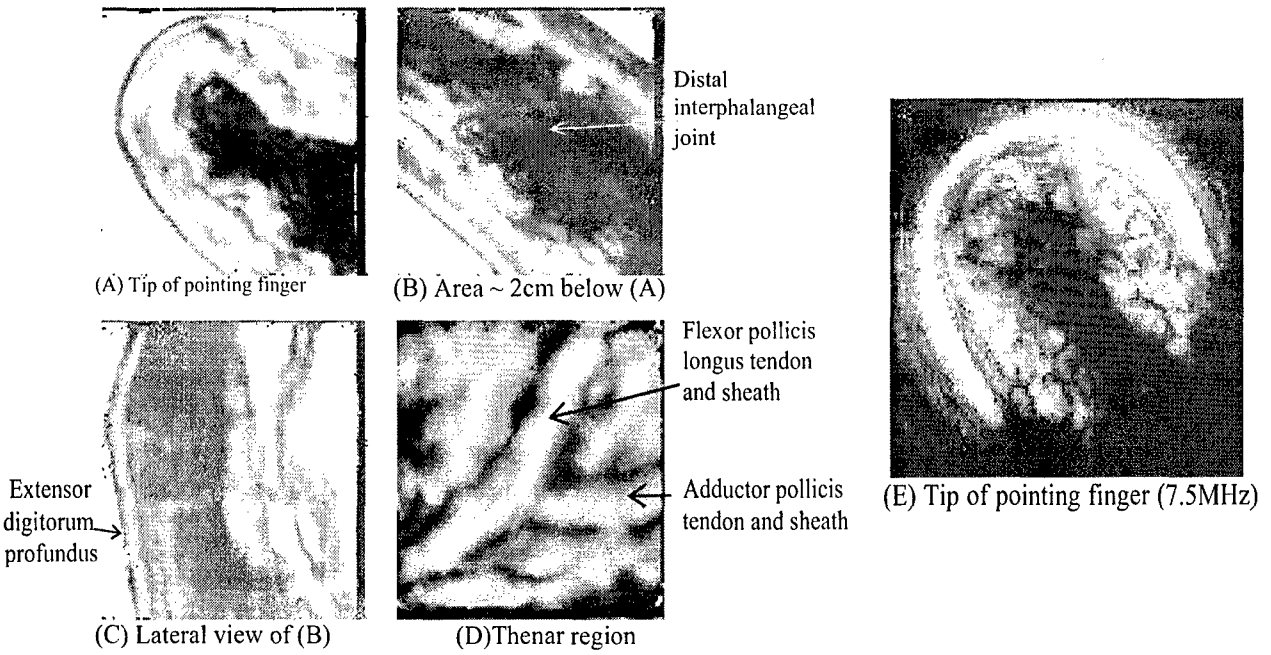

Figure 8. Four finger sample images (A-D) were taken by the ultrasound system operated at 5 MHz. (E) is a 7.5 MHz image of pointing finger tip which shows many small vessels and fibrotic tissues.

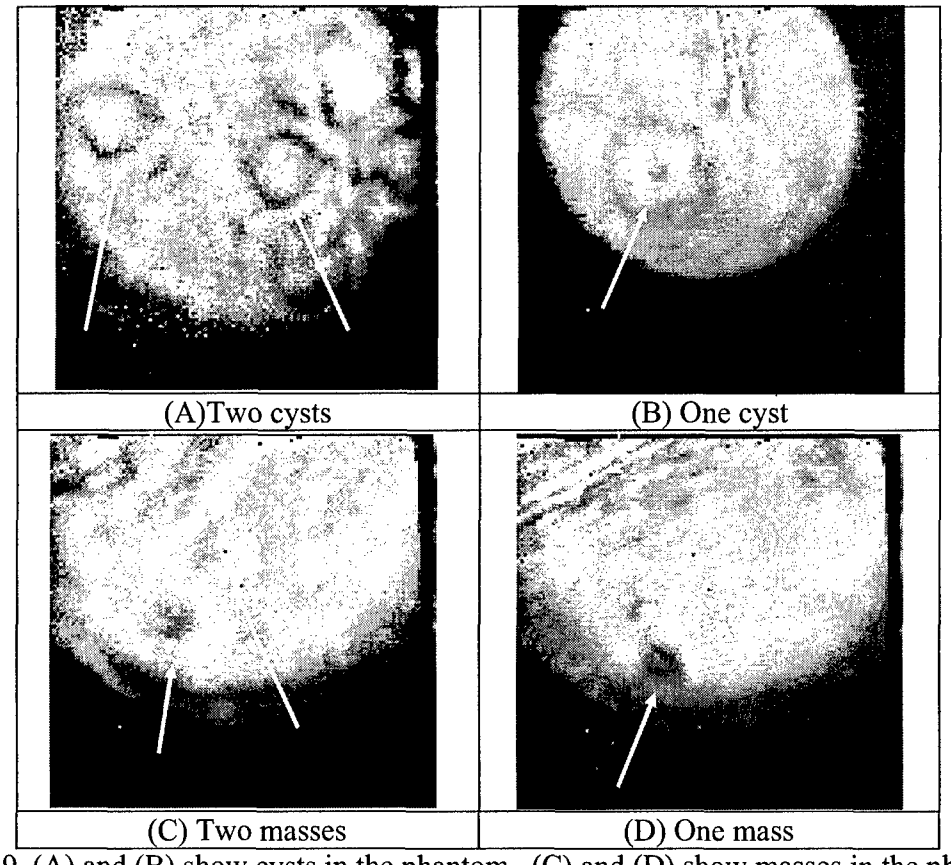

Figure 9. (A) and (B) show cysts in the phantom. (C) and (D) show masses in the phantom.

As shown in Figure 8, the device provides unusually clear delineation of tendons and the bony structures of the fingers including vessels and sublimis tendon around the profundus tendon. Thus, it is likely to become a low cost method of evaluating the integrity of the tendons of the extremities following trauma. Currently such assessment is made using physical examination, surgical exploration and/or MRI. Incomplete tendon injuries are difficult to detect by physical examination, but should be easy to see using this device. The device has sufficient penetration of the bones of the fingers such that it should be feasible to monitor the placement of surgical pins, in real time, without x-rays. Thus the system should be competitive with hand held fluoroscopes that are in some cases used for this purpose. The advantage of this system would be that one could at all times see the relationship of the tendons and vessels to the pins, whereas the hand held fluoroscope only allows the visualization of the bone and the pins.

In addition, the same 7.5MHz transducer was used to image a CIRS model 52 breast mimicking phantom. Several images were taken and four of them are shown in Figure 9. The CIRS model 52 phantom contains cysts and masses as well as some destructed structures which are clearly shown on these pictures

2.4. Reflective Imaging Mode for Bone Surface Imaging

We have also performed a pilot study to demonstrate the feasibility of reflective ultrasound imaging using cracked beef ribs. We used a hammer to traumatize the beef ribs. The ribs were imaged with the muscle layer intact. These sample ribs were placed in a water tank with the US camera set up in the pulse-echo mode using a 1-inch diameter transducer (equivalent to 0.7" square region) operating at 5 MHz. Figure 10 shows the set-up of the experiment in water tank. The cracked rib is shown at the left bottom region of Figure 10.

Reflective images resulting from these tests are shown in Figure 11. Note that the cracks on the rib are clearly visible in Figures 11 (A), (B), and (D). We are particularly encouraged by the visibility of fine cracks in Figure 11(A). Dark lines on the images indicate that the regions lack reflecting ultrasound signals. It is estimated that the finest lines in the fracture are approximately 500 μm. This initial study indicates that it is likely that the new ultrasound imaging technology can be employed to aid to detect fine rib fractures in humans.

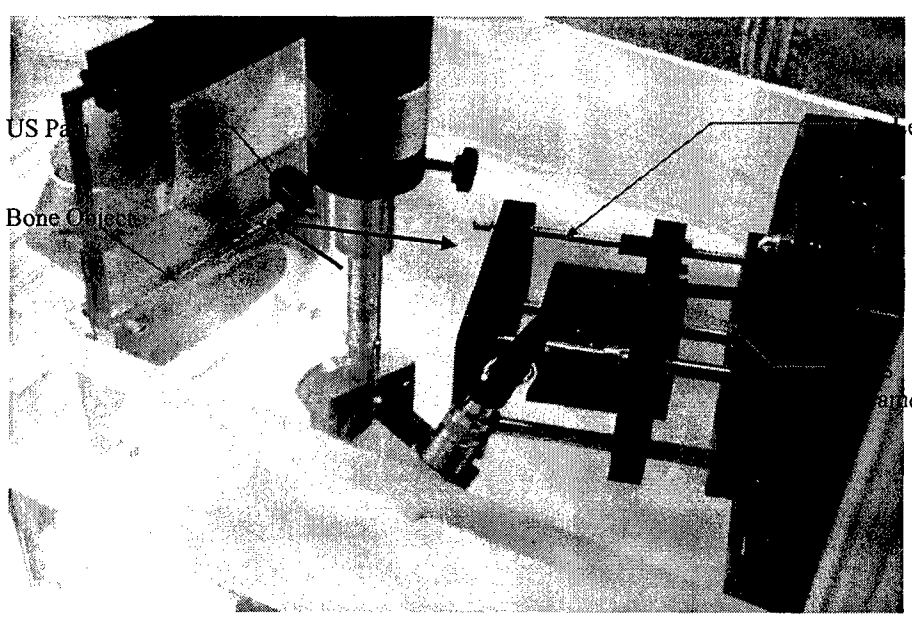

Figure 10. Ultrasound camera set-up using reflective geometry

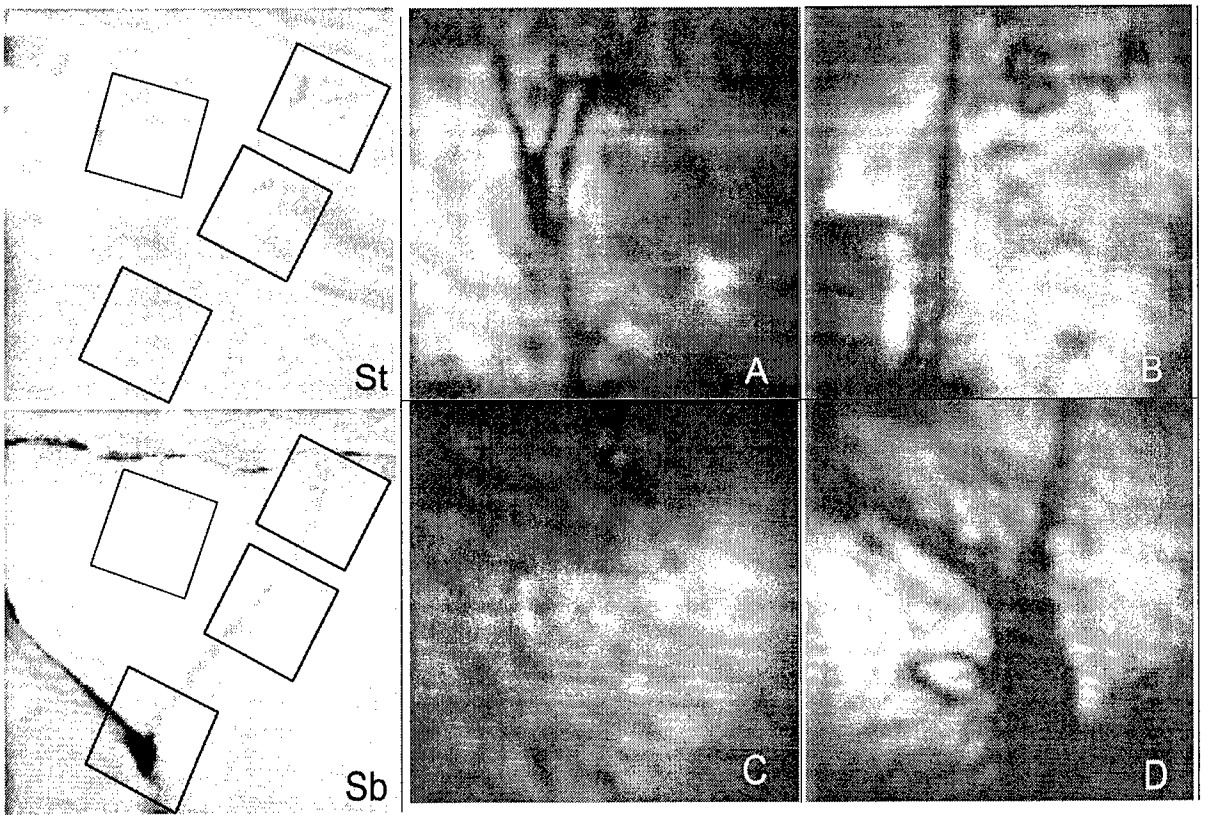

Figure 11. (St): A piece of beef rib covered with its original tissue undissected. **(Sb)**: The same cracked beef rib after the muscle is removed. The other four images shown here **(A), (B), (C) and (D)** were obtained by placing **(St)** (the rib with muscle) and imaged with the laboratory prototype as shown in Figure 9. All four images were taken by adjusting the focus of the lens at depth of 0.5 cm. Note that image (A) shows three fine cracks that are barely visible on the upper right corner of the bone surface image **(Sb)**. The scale ratio between ultrasound images and beef rib pictures is approximately 4:1 in one dimension.

CONCLUSIONS

We have established a laboratory prototype to investigate the potential medical applications of the PE-CMOS array. We found that this novel two-dimensional ultrasound sensing array can generate real-time, high-resolution, speckle-free attenuation images including subsurface structures in the human tissue. The array is responsive over a wide range of ultrasound frequencies, although most imaging is done using frequencies ranging from 1MHz to 15MHz. Substantial improvements have been made in the physical performance of the imaging system based on the newly developed chip (model I400).

In this study, we have also conducted a series of physical evaluation studies to investigate the performance of this prototype system and its clinical potential. We found that the spatial resolution of the system is approximately 350 μm and the dynamic range increased to 70dB. We also demonstrated that both high quality transmission and reflective ultrasound images can be generated using the PE-CMOS sensor. The reflective images of bone surface images clearly show fine bone fractures, which indicates the clinical implications of the new ultrasound system on musculo-skeletal applications. Since the system apparatus is quite simple and inexpensive and the

image resolution is much higher, this ultrasound attenuation imaging system has substantial clinical implications.

ACKNOWLEDGMENTS

This work was supported in part by an NIH/NIBIB Grants (No. EB002130) and US Army research grant (No. DAMD17-0101-0197).

REFERENCES

1. T.E. Trumble, N.B. Vedder, S.K. Benirschke, "Misleading fractures after profundus tendon avulsions: a report of six cases," Hand Surg [Am]. 1992 Sep;17(5):902-6.
2. R.C. Russell, D.A. Williamson, J.W. Sullivan, H. Suchy, O. Suliman, "Detection of foreign bodies in the hand," J Hand Surg [Am]. 1991 Jan;16(1):2-11.
3. B.D. Fornage, "Soft-tissue changes in the hand in rheumatoid arthritis: evaluation with US, Radiology. 1989 Dec;173(3):735-7.
4. S.B. Lo, D. Rich, M.E. Lasser, J. Kula, H. Zhao, R. Lasser, and M.T. Freedman, "A C-Scan Transmission Ultrasound Based on a Hybrid Microelectronic Sensor Array and Its Physical Performance," SPIE Proc. Med. Img. Vol. 4325, pp. 89-93, 2001.
5. A. Ishisaka, H. Ohara, and C. Honda, "A New Method of Analysis Edge Effect in Phase Contrast imaging with Incoherent X-rays," Optical Review, Vol. 7, No. 6, pp.566-572, 2000.

P 29-7

AN ATTENUATION-BASED ULTRASOUND SYSTEM USING A PIEZOELECTRIC SENSING MICROARRAY AND ITS POTENTIAL FOR IMAGING THE BREAST

Chu-Chuan Lin[a], Shih-Ching B. Lo, Ph.D[b], Marvin E. Lasser, Ph.D[a], Matthew T. Freedman, M.D[b], Yue Wang, Ph.D[a]

[a] Department of Electrical Engineering and Computer Science, The Catholic University of America, Washington, D.C. 20064

[b] Lombardi Cancer Research Center, Department of Radiology, Georgetown University Medical Center, Washington, D.C. 20007

Imagyn Inc., Silver Spring, Maryland 20910

Abstract

An attenuation based ultrasound system using C-scan geometry has been constructed based on a pixelated hybrid piezoelectric array that is capable of generating ultrasound images with fluoroscopic presentation. The array is made up of two components: a silicon readout or readout array and a piezoelectric material that is fabricated onto the array through semiconductor processing. The size of the array is 1 cm on each side. It consists of 128×128 pixel elements with 85 microns per pixel. The ultrasound source if it strikes the piezoelectric material is converted to an analog voltage that is digitized and processed by a standard commercial video electronics.

To generate real-time images, ultrasound is introduced into the object under study with a large unfocused plane wave source. The ultrasound wave transmits through the object and is attenuated and scattered. The device detects reflected as well as attenuated ultrasound energy which allows the use of an acoustic lens for focusing no detected energy from an object plane. The acoustic lens collects the transmitted energy and focuses it onto the microarray. Hence, a circular area covering 3 inches in diameter can be imaged into the sensor.

The images generated by the device appear no speckle with fluoroscopy-like presentation. The images show no obvious geometrical distortion. The experimental results indicated that the system has a spatial resolution of ~0.12 mm. It can detect less than 3mm simulated breast lesions with low differential contrast and an attenuation coefficient difference less than 0.07 dB/cm/MHz. Phase contrast of the lesion objects is also clearly visible. Based on this prototype, we have demonstrated a procedure for image guided breast biopsy. In addition, punctured needle tracks in a tissue were clearly observed. This implies the potential of observing the speculation of masses in vivo.

Introduction

Clinically, ultrasound has been used in screening dense breast regions and in distinguishing between cysts and solid masses. In many situations, it is also used as an image modality to guide needle biopsy of breast lesions. Recently Imperium Inc. has developed an ultrasound-receiving (piezoelectric) layer deposited onto a microarray chip through semiconductor processing (see Figure 1). The array is responsive over a wide range of ultrasound frequencies, although most imaging is done between 1MHz and 15MHz. In the training program we propose to use this novel two-dimensional ultrasound attenuation imaging system that creates real-time, high-resolution images of subsurface structures in the breast.

In order to generate attenuation images, ultrasound is introduced into the target under study with a large unfocused ultrasound plane wave. The ultrasound wave strikes the target and is attenuated and scattered. An acoustic lens collects the energy and focuses it onto the ultrasound-sensitive array. This high-resolution distortion-free ultrasound imaging system has unique potential for improved soft tissue diagnosis in general. We have also conducted a series of physical evaluation studies to investigate the performance of this prototype system and its clinical potential. A part of its physical performance, image quality, and clinical implications are reported in the following sections.

Material and Methods

The system operates by pulsing a commercial off-the-shelf ultrasonic spike pulser. A plane wave exits the target, scatters, exits the target and strikes the acoustic lens which collects the scattered energy and focuses it onto the array. The operation repeats 30 times per second. Standard video electronics and image processing are used to format the image for presentation to the user and perform real time image processing, either on a PC monitor or hand held LCD. Figure 3 shows the system architecture. Figure 4 is our laboratory device setting. The sensor microarray and the ultrasound source are located in the left side and right side of the water tank.

The evaluation study was performed in a closed water tank environment. The ultrasound was operated at a peak frequency of 5MHz using a broad band unfocused planar wave (1.5" spatial) transducer (Ametek Model No. SRP-040-050 S/N 001 MWS). The pulser was a SDI Imperium I-100 standard pulser S/N – 001. The hydrophone was provided by Specialty Engineering (Model GL-0400, SN G727). The hydrophone has a sensitivity of 22.4kPa/mV at 5MHz. The acoustic lens used was a two-element spheric 50mm diameter F/1 (Imperium 914 series). The camera contains an Imperium proprietary sensor array (Model I-110 S/N 013 Array S/N 17-58). In order to acquire the signal in real-time, the circuit signals were converted to video signals and digitally recaptured at 30 frames per pixel by a frame grabber at a rate of 1/30 second. An off the shelf frame grabber (Matrox Meteor II standard) was adapted in the system. These studies were performed using phantoms made by CIRS (Computerized Imaging Reference Systems, Inc., Norfolk, VA).

Correspondence: Chu-Chuan Lin, 18thin@cua.edu

Two sets of spheres were inserted into a background material (Zerdine™), whose density designed to simulate breast tissue. The density of the background material was 0.22 dB/cm/MHz. Each set consists of four spheres with different ultrasound attenuation: 0.60, 0.15, 0.5, and 0.8 dB/cm/MHz. The first set of spheres were 1mm in size and the second set of spheres were 5mm. Figure 5 shows the images of the 5mm spheres taken with the prototype system. The field of view of the prototype system is limited so two pictures were taken for this set of spheres. Figure 6 shows the images of the 3mm spheres. We also performed a quantitative measure using contrast-to-noise-ratios (CNR) for each sphere. The CNR was computed as follows

$$CNR = (\mu_o - b_o)/\sqrt{(\sigma_o^2 + \sigma_b^2)/2}$$

where μ_o and b_o are mean intensity values of foreground and background, respectively. The quantities σ_o and σ_b are the corresponding standard deviations. Table I and II list the results of CNRs for 5mm and 3mm spheres, respectively. In Figures 6 and 7, the edges of the cyst mimicking and tumor mimicking spheres are clearly observed with a phase contrast phenomenon. Figure 8 shows the ROIs and their intensities, and CNRs measures for the smallest clustered calcifications. Figure 9 , 10 and 11 shows the images taken from a set of fan lines.

The chip has some inactive pixels that show white dots in the image. As a part of image pre-processing, we first take a background image (without using pulses from the system). Then we apply a point detector filter to mark the locations of inactive pixels. After we located those inactive pixels, we took average value of the 4 adjacent pixels to represent the gray value of the inactive pixel. The results are shown in Figure 13.

We have also performed tests using breast phantoms containing simulated breast abnormalities including tumors and cysts. Again, each image was extracted from 1 single frame (1/30 seconds of the sequential images without post-processing. Figure 14 shows a sequence of needle biopsy images using a CIRS phantom (Model 52) acquired from the C-Scan prototype. The phantom has been used for training residents for sometime. A 2-cm tumor in the phantom was used as a model in the second part of the experiment. Figure 15 demonstrated several focal plane fields of the same detail obtained as one focuses from the edge into the center of the simulated. Each image contains a black boundary representing the region outside of the field of view of the transducer disk. Within this boundary is a lighter gray area which represents the background material of the phantom which surrounds the spherical details. The darker region in the center represents the spherical detail in the phantom. As we focus into the object, the cross section of the spherical object becomes larger, as expected, as one slices a sphere from its edge. The black linear streaks are the needle tracks. The white streaks are, we believe, based on a mammographic x-ray image areas of leakage of the material from the spherical objects.

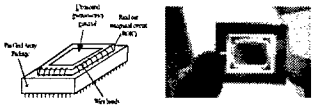

Figure 1. Schematic of array assembled array

Figure 2. 128 × 128 assembled array

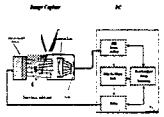

Figure 3. The prototype system configuration

Figure 4. Laboratory setting in a water tank

Detectablity of Masses

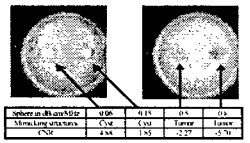

Sphere in dB/cm/MHz	0.06	0.15	0.5	0.8
Mimicking structures	Cyst	Cyst	Tumor	Tumor
CNR	4.64	1.85	-2.27	-5.70

Figure 5. The C-Scan images of four 5mm spheres using Zerdine™ background at 0.22 dB/cm/ MHz. (A) Cysts mimicking spheres with 0.06 dB/cm/MHz at the left and 0.15 dB/cm/MHz at the right. (B) Tumor mimicking spheres with 0.5 dB/cm/MHz at the left and 0.8 dB/cm/MHz at the right

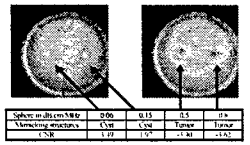

Sphere in dB/cm/MHz	0.06	0.15	0.5	0.8
Mimicking structures	Cyst	Cyst	Tumor	Tumor
CNR	1.69	1.93	-1.81	-4.67

Figure 6. The C-Scan images of four 3mm spheres using Zerdine™ background at 0.22 dB/cm/ MHz. (A) Cysts mimicking spheres with 0.06 dB/cm/MHz at the left and 0.15 dB/cm/MHz at the right, (B) Tumor mimicking spheres with 0.5 dB/cm/MHz at the left and 0.8 dB/cm/MHz at the right

Detectablity of Microcacifications

Figure 7. Images of the C-scan system for the three sets of clustered calcifications setting in breast tissue mimicking Zerdine™ (A)0.7-0.85mm clustered calcifications (B) 0.42-0.45mm clustered calcifications (C) 0.3-0.35mm clustered calcifications

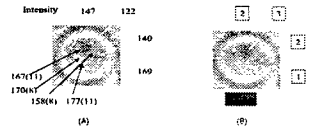

Figure 8. ROIs and their intensities and CNRs measures for the smallest clustered calcifications. (A) Four intensity measures for the calcifications upper-right corners and the intensity (noise level) measures at selected background areas (B) Estimated CNR values of the four calcifications.

Fan Line as a Test Target

(A) A fan pattern is constructed by 7 stainless steel wires. Each wire is 250 microns thick/wire.

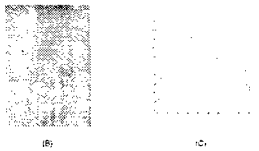

Figure 9. A fan-lines phantom is shown in (A), image of the fan-lines in (B), the inversed intensity profile in (C) at 0.22 mm spacing at the level indicated by the yellow line in (B).

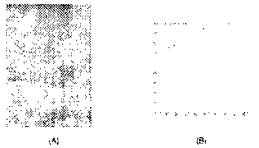

Figure 10.(A) Image of the fan-lines in Figure 10 (A), the inversed intensity profile in (C) at 0.36 mm spacing at the level indicated by the yellow line in (A)

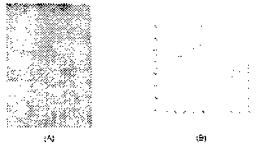

Figure 11.(A) Image of the fan-lines in Figure 9(A), the inversed intensity profile in (C) at 0.56 mm spacing at the level indicated by the yellow line in (A)

A C-Scan Image Sequence

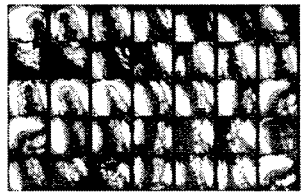

Figure 12. A C-scan image sequence of human finger

Compensation for Inactive Pixels

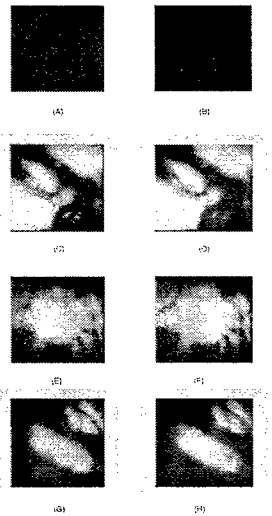

Figure13. A point detector was used to automatically detect inactive pixels followed by a compensation processing. (A) Background image without phase. (B) Filtered background image (C=F-G) Original test images (D=E+H) Fixed images.

Breast Biopsy Simulations

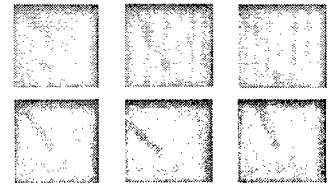

Figure 14. The above images were sampled from a sequence of 150 ultrasound images taken from 30 frames per second for five seconds of a CIRS breast phantom. The C-scan ultrasound focused on two small simulated masses and a biopsy needle about 4 cm below the surface.

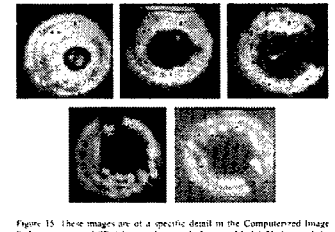

Figure 15. These images are of a specific detail in the Computerized Image Reference Systems (CIRS) breast ultrasound phantom Model 52, designed for tissue equivalent ultrasound needle biopsy training. These results imply the speculation of breast masses could be observable by the imaging device.

Conclusion And Discussion

In summary, we found the prototype system based on this hybrid microelectronic array that is capable of generating ultrasound images with fluoroscopy-like presentation and without speckle artifacts. The images show no obvious geometrical distortion. The resolution study indicates that a spatial resolution of ~320 microns was observable using a fan-line phantom and calcification phantom. The contrast resolution study indicate that the system is capable of differentiating objects 3mm in size with low differential contrast. The difference between the target and background materials in this experiment was as low as 0.07 dB/cm/MHz.

The potential for use in biopsy procedures is demonstrated through the imaging of breast phantoms with simulated tumors. The system is capable of imaging the area of interest in real-time. In addition, the image resolution and quality presented from the new device seem to outperform over the conventional ultrasound system in terms of inspection of mass speculation and size of microcalcifications. Clinical investigation of the system is in-progress.

Acknowledgments

This work was supported by the U.S. Army Medical Research and Material Command under DAMD17-01-1-0197 pre-doctoral award.